Photocontrolled activation of doubly ONB-protected small molecule benzimidazoles leads to cancer cell death

Manzoor Ahmad,[a,d] Naveen J. Roy,[a] Anurag Singh,[a,e] Debashis Mondal,[a,f] Abhishek Mondal,[a] Thangavel Vijayakanth,[b] Mayurika Lahiri,[c] and Pinaki Talukdar*[,a]

[a] Department of Chemistry, Indian Institute of Science Education and Research Pune, Dr. Homi Bhabha Road, Pashan, Pune 411008, Maharashtra, India.

[b] The Shmunis School of Biomedicine and Cancer Research, George S. Wise Faculty of Life Sciences, Tel Aviv University, Tel Aviv 6997801, Israel.

[c] Department of Biology, Indian Institute of Science Education and Research Pune, Dr. Homi Bhabha Road, Pashan, Pune 411008, Maharashtra, India.

[d] Present Address: Chemistry Research Laboratory, Mansfield Road, Oxford, OX1 3TA, UK.

[e] Present Address: Universite´ libre de Bruxelles (ULB), Ecole polytechnique de Bruxelles, Engineering Molecular NanoSystems, Avenue Franklin Roosevelt 50, 1050 Brussels, Belgium.

[f] Present Address: Faculty of Chemistry, Biological and Chemical Research Centre, University of Warsaw, Zwirkii Wigury 101, Warsaw 02-089, Poland.

E-mail: ptalukdar@iiserpune.ac.in

Table of Contents:

I. General methods.

All chemical reactions were carried out under a nitrogen atmosphere. All reagents and solvents for synthesis were purchased from commercial sources (Sigma-Aldrich and Spectrochem), and used without further purification. The column chromatography was carried out using Merck silica gel (100-200 mesh size). The thin layer chromatography was performed on Merck silica gel 60-F254 plates. Egg yolk phosphatidylcholine (EYPC) as a solution of chloroform (25 mg/mL), mini extruder, and polycarbonate membrane of 100 nm and 200 nm were purchased from Avanti Polar Lipid. HEPES, HPTS, lucigenin, NaOH, Sephadex G-50, Triton X-100, valinomycin, and all inorganic salts were obtained as molecular biology grade from Sigma Aldrich.

II. Physical measurements.

All the NMR spectra were recorded on a 400 MHz spectrophotometer. The residual solvent signals were considered as an internal reference (δ_H = 7.26 ppm for $CDCl_3$, δ_H = 2.50 for DMSO-d_6, and δ_H = 1.94 for CD_3CN) to calibrate spectra. The chemical shifts were reported in ppm. Following abbreviations were used to indicate multiplicity patterns m: multiplet, s: singlet, d: doublet, dd: doublet of doublets, td: triplet of doublets, ddd: doublet of doublet of doublets. Coupling constants were measured in Hz. Infra-red (IR) spectra were measured in cm^{-1} using an FT–IR spectrometer. Melting points were measured on a micro melting point apparatus and are uncorrected. High-resolution mass spectra (HRMS) were recorded on an electrospray ionization time-of-flight (ESI-TOF) mass spectrometer. Fluorescence experiments were recorded on a Fluoromax-4 instrument from Horiba equipped with an injector port and magnetic stirrer. All buffer solutions were prepared in autoclaved water. Adjustment of the pH of buffer solutions was made using a pocket pH meter purchased from Hanna instruments. The extravesicular dye was removed by performing gel chromatography using Sephadex G-50. The fluorescence data were processed using OriginPro 8.5. ChemDraw 21.0.0 software was used for drawing structures and processing figures. UV-vis spectra were recorded on a Shimadzu UV-2600 UV-Vis spectrophotometer. Chloride ion efflux was measured using a Thermo Scientific Orion Chloride ion plus ISE connected to a Fisherbrand AB 250 pH/ISE meter for recording chloride concentration in ppm.

III. Synthesis.

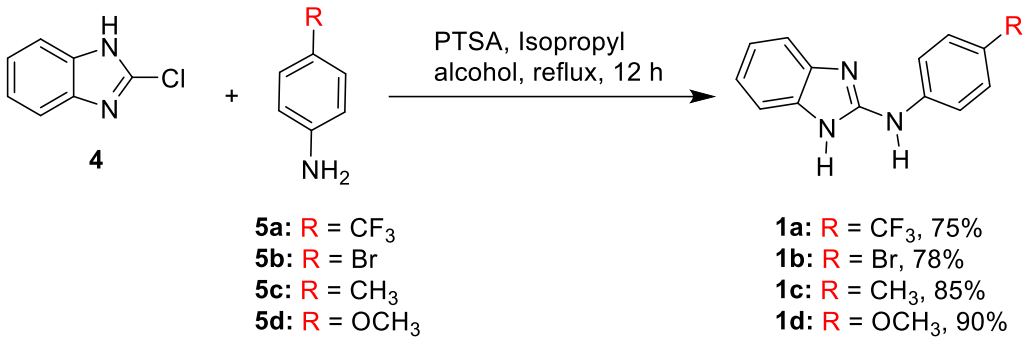

Scheme 1. Synthesis of the desired active transporters **1a–1d**.

Experimental procedures.

General procedure for the synthesis of 1a–1d: In a 50 mL round bottom flask, 2-chloro-1*H*-benzimidazole **4** (1 equiv.) was dissolved in 20 mL of isopropyl alcohol. To this solution, corresponding aromatic aniline derivatives **5a**–**5d** (1 equiv.) and *p*-toluenesulfonic acid (1 equiv.) were added. The mixture was stirred at 105 ^{o}C for 12 h. After the completion of the reaction monitored by TLC, the solvent was evaporated, and the crude mixture was extracted with ethyl acetate (3 × 30 mL) and sodium bicarbonate solution. The organic layer was dried with anhydrous sodium sulfate, filtered, and concentrated under reduced pressure using a rotary evaporator to give the crude product. The residue was then purified by column chromatography over 100–200 mesh silica gel to furnish **1a**–**1d** in 75–90% yield.

***N-(4-(trifluoromethyl)phenyl)-1H-benzo[d]imidazol-2-amine, $C_{14}H_{10}F_3N_3$ (1a)*:** Synthesized by reacting 2-chloro-1*H*-benzimidazole **4** (200 mg, 1.31 mmol, 1 equiv.) with 4-bromoanilene (225 mg, 1.31 mmol, 1 equiv.). The crude product was purified by column chromatography over 100–200 mesh silica gel (*Eluent*: EtOAc : petroleum ether 3:7 v/v) to furnish **1a** as white solid (272 mg, 75%). **^{1}H NMR (400 MHz, DMSO-*d*6):** δ 11.11 (s, 1H), 9.91 (s, 1H), 7.97 (d, J = 8.6 Hz, 2H), 7.66 (d, J = 8.6 Hz, 2H), 7.36 (dd, J = 32.1, 7.5 Hz, 2H), 7.14 – 6.94 (m, 2H); **^{13}C NMR (101 MHz, DMSO-d_6):** δ 162.5, 153.9, 146.4, 145.9, 131.0, 125.3, 114.8, 94.8, 68.1, 31.2, 19.2, 13.8; **IR (Neat, v/cm^{-1}):** 3368, 3143, 2305, 1574, 1461, 1322, 1246, 1158; **HRMS** (ESI^{+}) *m/z*: [M + H]$^{+}$ calcd. for $C_{14}H_{10}F_3N_3$: 278.0900, found: 278.0902.

N-((p-bromo)phenyl)-1H-benzo[d]imidazol-2-amine, $C_{13}H_{10}BrN_3$ (1b): Synthesized by reacting 2-chloro-1*H*-benzimidazole **4** (200 mg, 1.31 mmol, 1 equiv.) with 4-(trifluoromethyl)aniline (211 mg, 1.31 mmol, 1 equiv.). The crude product was purified by column chromatography over 100–200 mesh silica gel (*Eluent*: EtOAc : petroleum ether 4:6

v/v) to furnish **1b** as white solid (294 mg, 78%); **^{1}H NMR (400 MHz, DMSO-*d*6):** δ 10.99 (s, 1H), 9.60 (s, 1H), 7.76 (d, J = 8.9 Hz, 2H), 7.47 (d, J = 8.9 Hz, 2H), 7.33 (d, J = 6.5 Hz, 2H), 7.10–6.89 (m, 2H); **^{13}C NMR (101 MHz, DMSO-d_6):** δ 150.5, 140.7, 131.9, 120.6, 119.4, 116.4, 112.1, 110.1; **IR (Neat, ν/cm^{-1}):** 3365, 3140, 2307, 1574, 1464, 1322, 1248, 1158; **HRMS** (ESI$^+$) *m/z*: [M + H]$^+$ calcd. for $C_{13}H_{10}BrN_3$: 288.0131, found: 288.0136.

***N-(p-tolyl)-1H-benzo[d]imidazol-2-amine, $C_{14}H_{13}N_3$ (1c)*:** Synthesized by reacting 2-chloro-1*H*-benzimidazole **4** (200 mg, 1.31 mmol, 1 equiv.) with *p*-toluidine (140 mg, 1.31 mmol, 1 equiv.). The crude product was purified by column chromatography over 100–200 mesh silica gel (*Eluent*: EtOAc : petroleum ether 3:7 v/v) to furnish **1a** as white solid (248 mg, 85%); **^{1}H NMR (400 MHz, DMSO-d_6):** δ 10.84 (s, 1H), 9.26 (s, 1H), 7.63 (d, J = 8.5 Hz, 2H), 7.30 (dd, J = 5.8, 3.3 Hz, 2H), 7.12 (d, J = 8.2 Hz, 2H), 7.07–6.92 (m, 2H), 2.26 (s, 3H); **^{13}C NMR (101 MHz, DMSO-d_6):** δ 151.2, 138.8, 129.7, 129.6, 120.4, 117.6, 20.81; **IR (Neat, ν/cm^{-1}):** 3368, 3144, 2305, 1577, 1466, 1322, 1250, 1158; **HRMS** (ESI$^+$) *m/z*: [M + H]$^+$ calcd. for $C_{14}H_{13}N_3$: 224.1183, found: 224.1186.

***N-(4-methoxyphenyl)-1H-benzo[d]imidazol-2-amine, $C_{14}H_{13}N_3O$ (1d)*:** Synthesized by reacting 2-chloro-1*H*-benzimidazole **4** (200 mg, 1.31 mmol, 1 equiv.) with 4-methoxyaniline (161 mg, 1.31 mmol, 1 equiv.). The crude product was purified by column chromatography over 100–200 mesh silica gel (*Eluent*: EtOAc : petroleum ether 4:6 v/v) to furnish **1a** as white solid (202 mg, 90%); **^{1}H NMR (400 MHz, DMSO-d_6):** δ 10.81 (s, 1H), 9.15 (s, 1H), 7.64 (d, J = 9.0 Hz, 2H), 7.27 (dd, J = 5.7, 3.3 Hz, 2H), 6.96 (dd, J = 5.8, 3.2 Hz, 2H), 6.91 (d, J = 9.0 Hz, 2H), 3.73 (s, 3H); **^{13}C NMR (101 MHz, DMSO-d_6)**: δ 154.1, 151.6, 134.6, 119.3, 114.5, 55.6; **IR (Neat, ν/cm^{-1}):** 3372, 3145, 2305, 1577, 1461, 1320, 1246, 11555; **HRMS** (ESI$^+$) *m/z*: [M + H]$^+$ calcd. for $C_{14}H_{13}N_3O$: 240.1132, found: 240.1137.

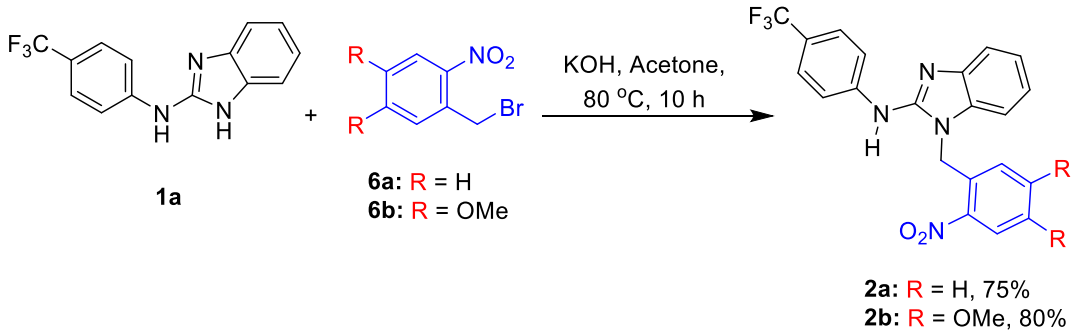

Scheme 2. Synthesis of the desired mono-ONB protected compounds **2a** and **2b**.

General procedure for the synthesis of mono-ONB protected procarriers 2a and **3a:** In a 50 mL round-bottomed flask, **1a** (1 equiv.) was dissolved in acetone 10 mL followed by the

addition of either **6a** or **6b** (1.0 equiv). A catalytic amount of KOH was added to the reaction mixture. This reaction mixture was stirred for 10 h at 80 ºC using an oil bath. After the completion of the reaction, the solvent was evaporated through a rotary evaporator, and the crude mixture was extracted with ethyl acetate (3 × 30 mL). The organic layer was dried with anhydrous sodium sulfate, filtered, and concentrated under reduced pressure to give the crude product. The residue was then purified by column chromatography over 100–200 mesh silica gel to furnish **2a** and **3a** in 75% and 80% yield, respectively.

***1-(2-nitrobenzyl)-N-(4-(trifluoromethyl)phenyl)-1H-benzo[d]imidazol-2-amine, $C_{21}H_{15}F_3N_4O_2$ (2a)*:** Synthesized by reacting *N*-(4-(trifluoromethyl)phenyl)-1*H*-benzo[d]imidazol-2-amine **1a** (100 mg, 0.36 mmol, 1 equiv.) with 1-(bromomethyl)-2-nitrobenzene **6a** (78 mg, 0.36 mmol, 1 equiv.). The crude product was purified by column chromatography over 100–200 mesh silica gel (*Eluent*: EtOAc : petroleum ether 1:9 v/v) to furnish **2a** as a white solid (111 mg, 75%). **^{1}H NMR (400 MHz, DMSO-d_6):** δ 9.50 (s, 1H), 8.27 (d, J = 9.4 Hz, 1H), 8.04 (d, J = 8.4 Hz, 2H), 7.68 (d, J = 8.7 Hz, 2H), 7.64–7.48 (m, 3H), 7.32 (d, J = 7.9 Hz, 1H), 7.16 (t, J = 7.5 Hz, 1H), 7.06 (t, J = 7.5 Hz, 1H), 6.47 (d, J = 6.5 Hz, 1H), 5.96 (s, 2H); **^{13}C NMR (101 MHz, $CDCl_3$):** δ 142.9, 140.3, 134.7, 133.4, 131.2, 129.3, 128.2, 126.4, 125.8, 125.6 (q, big), 124.7 (q, small)122.9, 122.0, 118.5, 117.4, 108.3, 43.7; **IR (Neat, v/cm^{-1}):** 3395, 3231, 3000, 2315, 1600, 1522, 1450, 1317, 1271; **HRMS** (ESI$^+$) *m/z*: $[M + H]^+$ calcd. for $C_{21}H_{15}F_3N_4O_2$: 413.1220, found: 413.1224.

***N,1-bis(2-nitrobenzyl)-N-(4-(trifluoromethyl)phenyl)-1H-benzo[d]imidazol-2-amine-N-(4-(trifluoromethyl)phenyl)-1H-benzo[d]imidazol-2-amine-1-(bromomethyl)-2-nitrobenzene (1/1/1), $C_{28}H_{20}F_3N_5O_4$ (3a)*:** Synthesized by reacting *N*-(4-(trifluoromethyl)phenyl)-1*H*-benzo[d]imidazol-2-amine **1a** (100 mg, 0.36 mmol, 1 equiv.) with 1-(bromomethyl)-2-nitrobenzene **6b** (155 mg, 0.72 mmol, 1 equiv.). The crude product was purified by column chromatography over 100–200 mesh silica gel (*Eluent*: EtOAc : petroleum ether 3:7 v/v) to furnish **3a** as a white solid (90 mg, 80%). **^{1}H NMR (400 MHz, $CDCl_3$):** δ 7.98 (ddd, J = 12.6, 7.9, 1.6 Hz, 2H), 7.75 (d, J = 9.6 Hz, 1H), 7.67 (d, J = 8.8 Hz, 1H), 7.51–7.44 (m, 1H), 7.41–7.29 (m, 4H), 7.29 – 7.23 (m, 3H), 7.15 (d, J = 7.4 Hz, 1H), 6.80 (d, J = 8.4 Hz, 2H), 6.64 (d, J = 6.2 Hz, 1H), 5.44 (s, 2H), 5.34 (s, 2H); **^{13}C NMR (101 MHz, $CDCl_3$):** δ 148.3, 147.0, 141.2, 135.0, 133.9, 133.6, 132.6, 130.1, 128.7, 128.5, 127.7, 126.8, 125.6 (q, small)125.2, 123.3, 123.1, 122.5 (q, big) 119.8, 119.6, 54.5, 45.0; **IR (Neat, v/cm^{-1}):** 2924, 2308, 1679, 1608, 1520, 1442, 1323, 1160; **HRMS** (ESI$^+$) *m/z*: $[M + H]^+$ calcd. for $C_{21}H_{15}F_3N_4O_2$: 548.1541, found: 548.1551.

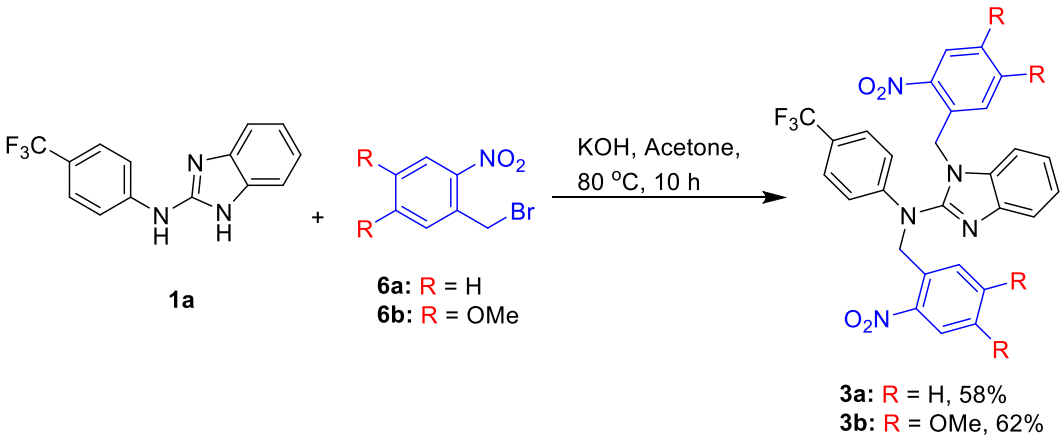

Scheme 3. Synthesis of the di-ONB protected compounds **3a** and **3b**.

General procedure for the synthesis of doubly-ONB protected compounds 2b and **3b:** In a 50 mL round-bottomed flask, **1a** (1 equiv.) was dissolved in 10 mL of acetone, followed by the addition of either **6a** or **6b** (2.0 equiv.). A catalytic amount of KOH was added to the reaction mixture. This reaction mixture was stirred for 10 h at 80 °C using an oil bath. After the completion of the reaction, the solvent was evaporated through a rotary evaporator, and the crude mixture was extracted with ethyl acetate (3 × 30 mL). The organic layer was dried with anhydrous sodium sulfate, filtered, and concentrated under reduced pressure to give the crude product. The residue was then purified by column chromatography over 100–200 mesh silica gel to furnish **2a** and **2b** in 80% and 62% yield, respectively.

***1-(4,5-dimethoxy-2-nitrobenzyl)-N-(4-(trifluoromethyl)phenyl)-1H-benzo[d]imidazol-2-amine, $C_{23}H_{19}F_3N_4O_4$ (2b)*:** Synthesized by reacting *N*-(4-(trifluoromethyl)phenyl)-1*H*-benzo[*d*]imidazol-2-amine **1a** (100 mg, 0.36 mmol, 1 equiv) with 1-(bromomethyl)-4,5-dimethoxy-2-nitrobenzene **6a** (99 mg, 0.36 mmol, 2 equiv). The crude product was purified by column chromatography over 100–200 mesh silica gel (*Eluent*: EtOAc : petroleum ether 1:9 v/v) to furnish **2b** as a white solid (136 mg, 80%). **^{1}H NMR (400 MHz, DMSO-d_6):** δ 9.47 (s, 1H), 8.12–7.97 (m, 2H), 7.81 (s, 1H), 7.67 (d, J = 8.6 Hz, 2H), 7.53 (dt, J = 7.8, 0.9 Hz, 1H), 7.29 (dt, J = 7.9, 0.9 Hz, 1H), 7.15 (td, J = 7.6, 1.2 Hz, 1H), 7.06 (ddd, J = 8.4, 7.4, 1.2 Hz, 1H), 5.92 (s, 2H), 5.84 (s, 1H), 3.86 (s, 3H), 3.31 (s, 3H); **^{13}C NMR (101 MHz, $CDCl_3$):** δ 149.2, 139.7, 133.5, 126.6,124.7 (q), 123.7 (q), 122.7, 121.7, 118.0, 109.1, 108.5, 108.0, 56.3, 43.8; **IR (Neat, v/cm^{-1}):** 3392, 3231, 3101, 2307, 1608, 1522, 1447, 1317, 1270; **HRMS** (ESI$^+$) *m/z*: $[M + H]^+$ calcd. for $C_{21}H_{15}F_3N_4O_2$: 473.1432, found: 473.1434.

***N,1-bis(4,5-dimethoxy-2-nitrobenzyl)-N-(4-(trifluoromethyl)phenyl)-1H-benzo[d]imidazol-2-amine, $C_{32}H_{28}F_3N_5O_8$ (3b)*:** Synthesized by reacting *N*-(4-(trifluoromethyl)phenyl)-1*H*-

benzo[*d*]imidazol-2-amine **1a** (100 mg, 0.36 mmol, 1 equiv.) with 1-(bromomethyl)-4,5-dimethoxy-2-nitrobenzene **6b** (199 mg, 0.72 mmol, 2 equiv.). The crude product was purified by column chromatography over 100–200 mesh silica gel (*Eluent*: EtOAc : petroleum ether 3:7 v/v) to furnish **3b** as a white solid (142 mg, 62%). **^{1}H NMR (400 MHz, $CDCl_3$):** δ 7.73 (d, J = 7.1 Hz, 1H), 7.57 (d, J = 9.7 Hz, 2H), 7.38–7.30 (m, 4H), 7.29 (dd, J = 3.6, 1.5 Hz, 1H), 7.25 (dd, J = 7.3, 1.2 Hz, 1H), 7.18 (d, J = 7.1 Hz, 1H), 6.82 (d, J = 8.4 Hz, 2H), 5.90 (s, 1H), 5.46 (s, 2H), 5.35 (s, 2H), 3.91 (d, J = 6.8 Hz, 6H), 3.80 (s, 3H), 3.35 (s, 3H); **^{13}C NMR (101 MHz, $CDCl_3$):** δ 153.6, 153.3, 152.4, 148.4, 148.0, 140.5, 139.6, 128.0 (q), 126.8, 125.3 (q), 124.8 (q), 123.5, 123.2, 122.6, 119.6, 119.0 , 112.43, 109.7, 109.0, 108.4, 108.3, 56.5, 56.4, 56.0, 54.2, 45.2; **IR (Neat, v/cm^{-1}):** 2923, 2310, 1588, 1512, 1447, 1323, 1267, 1213; **HRMS** (ESI$^+$) *m/z*: $[M + H]^+$ calcd. for $C_{21}H_{15}F_3N_4O_2$: 668.1963, found: 668.1970.

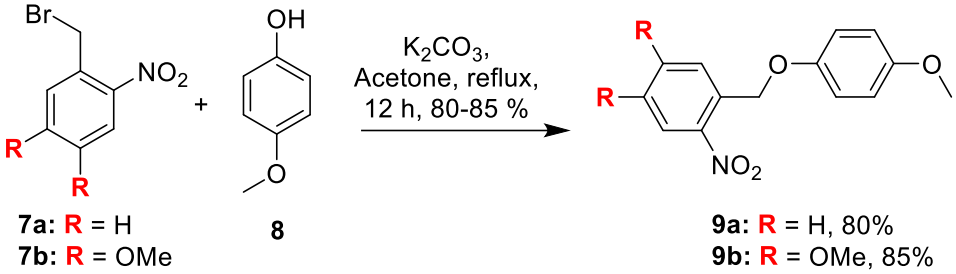

Scheme 4. Synthesis of the desired control compounds **9a** and **9b**.

General procedure for the synthesis of control compounds 9a and **9b:** In a 50 mL round-bottomed flask, 4-methoxy phenol **8** (1 equiv.) and K_2CO_3 (2 equiv) were dissolved in acetone (10 mL), followed by the addition of *o*-nitro-bromobenzyl compounds **7a** or **7b** (1.0 equiv.). The reaction mixture was stirred for 12 h at 80 ^{o}C using an oil bath. After the completion of the reaction, the solvent was evaporated through a rotary evaporator, and the crude mixture was extracted with ethyl acetate (3 × 30 mL). The organic layers were dried with anhydrous sodium sulfate, filtered, and concentrated under reduced pressure to give the crude product. The crude residue was then purified by column chromatography over 100–200 mesh silica gel to furnish **9a** and **9b** in 80% and 85% yield, respectively.

***1-((4-methoxyphenoxy)methyl)-2-nitrobenzene, $C_{14}H_{13}NO_4$ (9a)*:** Synthesized by reacting 4-methoxyphenol **8** (57 mg, 0.46 mmol, 1 equiv) with 1-(bromomethyl)-2-nitrobenzene **7a** (100 mg, 0.46 mmol, 1 equiv). The crude product was purified by column chromatography over 100–200 mesh silica gel (*Eluent*: EtOAc : petroleum ether 1:9 v/v) to furnish **9a** as a white solid (96 mg, 80%). **^{1}H NMR (400 MHz, $CDCl_3$):** δ 8.16 (dd, J = 8.2, 1.3 Hz, 1H), 7.91 (dd,

J = 7.9, 1.2 Hz, 1H), 7.68 (td, *J* = 7.6, 1.3 Hz, 1H), 7.54–7.43 (m, 1H), 6.99–6.81 (m, 4H), 5.44 (s, 2H), 3.77 (s, 3H); **^{13}C NMR (101 MHz, $CDCl_3$):** δ 154.3, 152.3, 134.3, 133.9, 128.6, 128.2, 124.9, 115.9, 114.8, 67.5, 55.7; **IR (Neat, ν/cm^{-1}):** 2923, 2310, 1588, 1512, 1447, 1323, 1267, 1213; **HRMS** (ESI^+) *m/z*: $[M + H]^+$ calcd. for $C_{21}H_{15}F_3N_4O_2$: 260.0917, found: 260.0930.

***1,2-dimethoxy-4-((4-methoxyphenoxy)methyl)-5-nitrobenzene, $C_{16}H_{17}NO_6$ (9b)*:** Synthesized by reacting 4-methoxyphenol **8** (45 mg, 0.36 mmol, 1 equiv) with 1-(bromomethyl)-4,5-dimethoxy-2-nitrobenzene **9b** (100 mg, 0.36 mmol, 1 equiv). The crude product was purified by column chromatography over 100–200 mesh silica gel (*Eluent*: EtOAc : petroleum ether 1:9 v/v) to furnish **9b** as a white solid (98 mg, 85%). **^{1}H NMR (400 MHz, $CDCl_3$):** δ 7.76 (s, 1H), 7.36 (d, *J* = 0.9 Hz, 1H), 6.94 (d, *J* = 9.2 Hz, 2H), 6.85 (d, *J* = 9.2 Hz, 2H), 5.44 (d, *J* = 0.8 Hz, 2H), 3.96 (d, *J* = 2.4 Hz, 6H), 3.77 (s, 3H); **^{13}C NMR (101 MHz, $CDCl_3$):** δ 154.4, 153.9, 152.2, 147.8, 139.0, 129.9, 116.0, 114.8, 109.4, 107.9, 67.8, 56.4, 56.3, 55.7; **IR (Neat, ν/cm^{-1}):** 2923, 2310, 1588, 1512, 1447, 1323, 1267, 1213; **HRMS** (ESI^+) *m/z*: $[M + H]^+$ calcd. for $C_{21}H_{15}F_3N_4O_2$: 320.1128, found: 320.1126.

IV. NMR spectra.

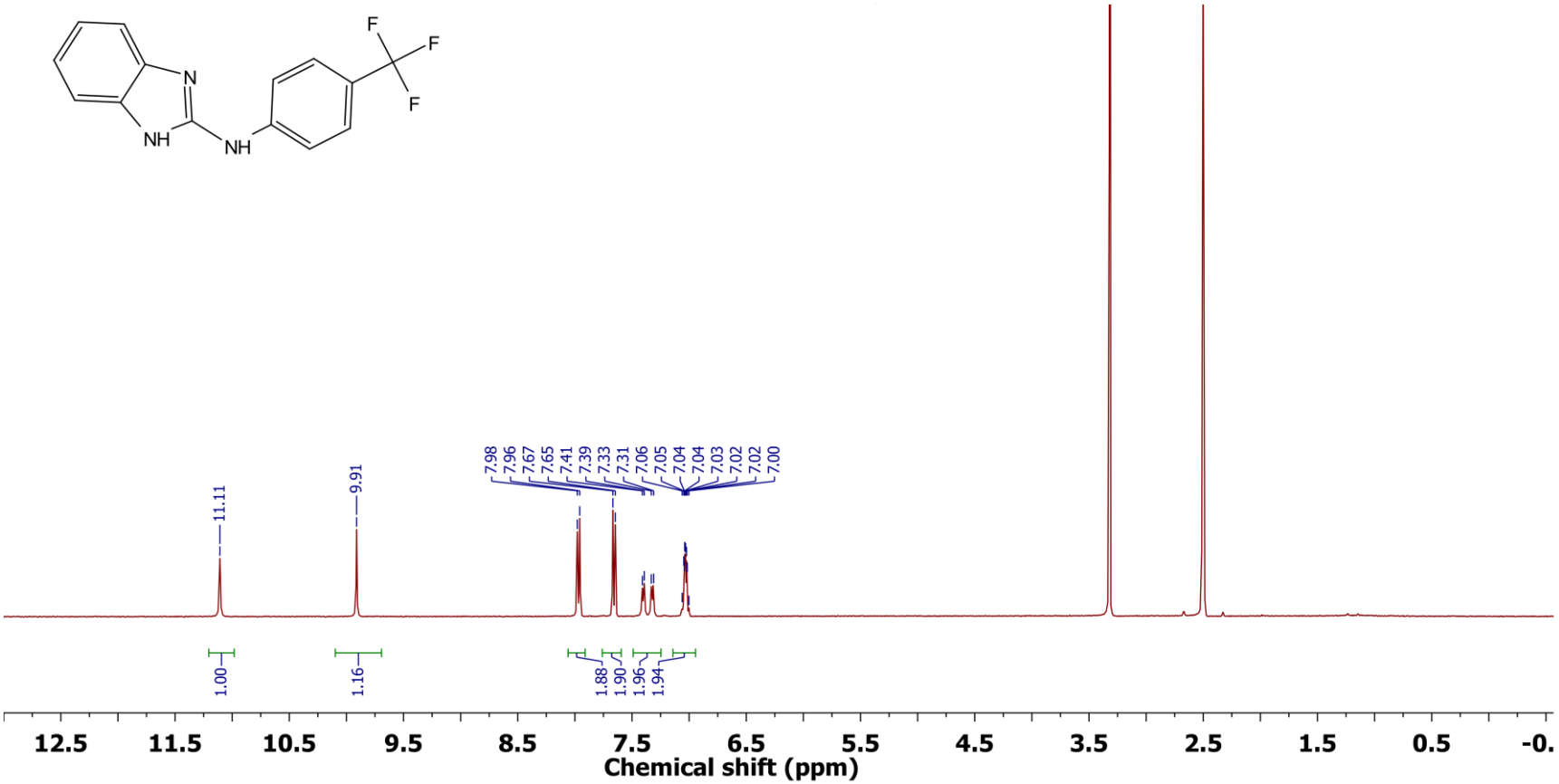

Fig. S1 ^{1}H NMR spectrum (400 MHz) of **1a** in DMSO-d_6 at room temperature.

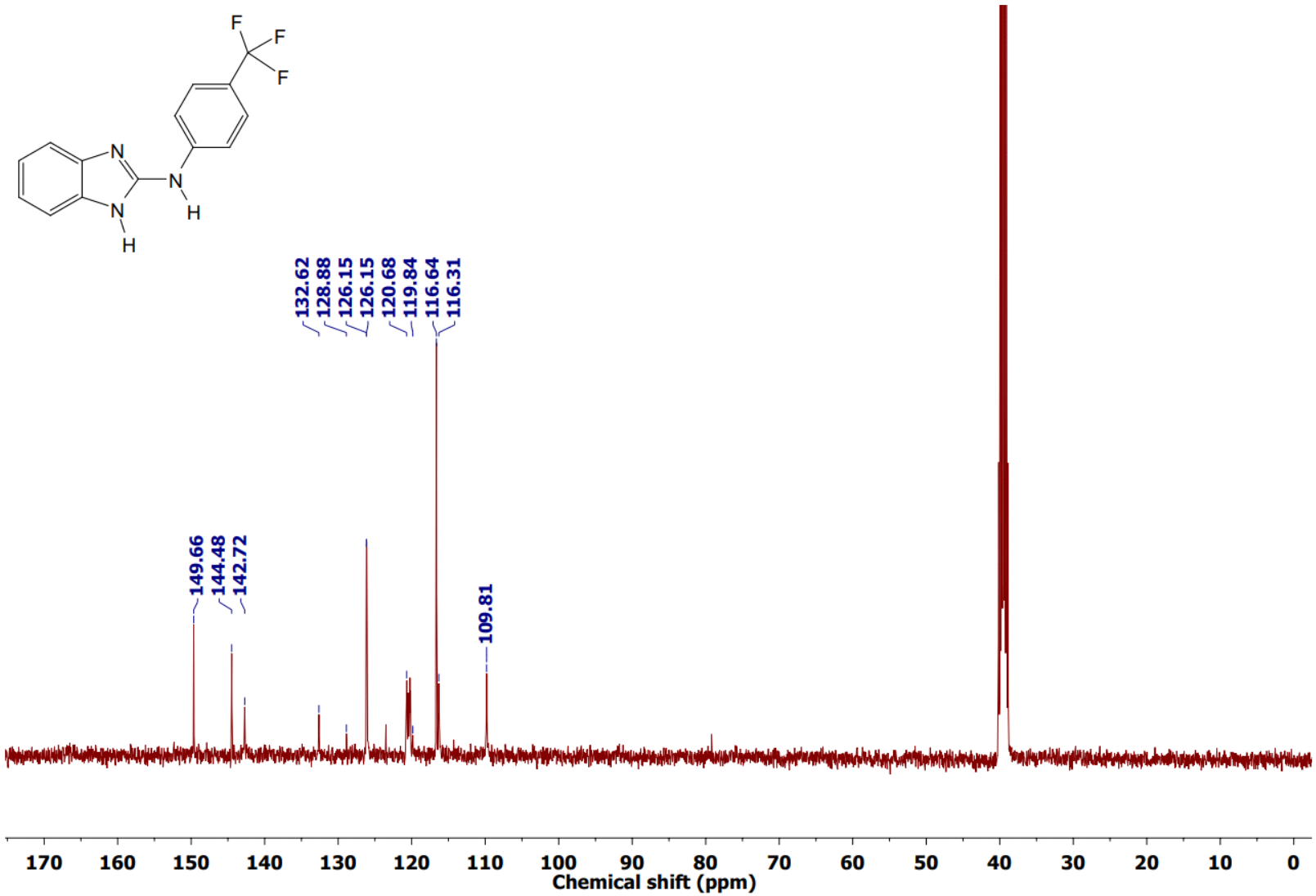

Fig. S2 ^{13}C NMR spectrum (101 MHz) of **1a** in DMSO-d_6 at room temperature.

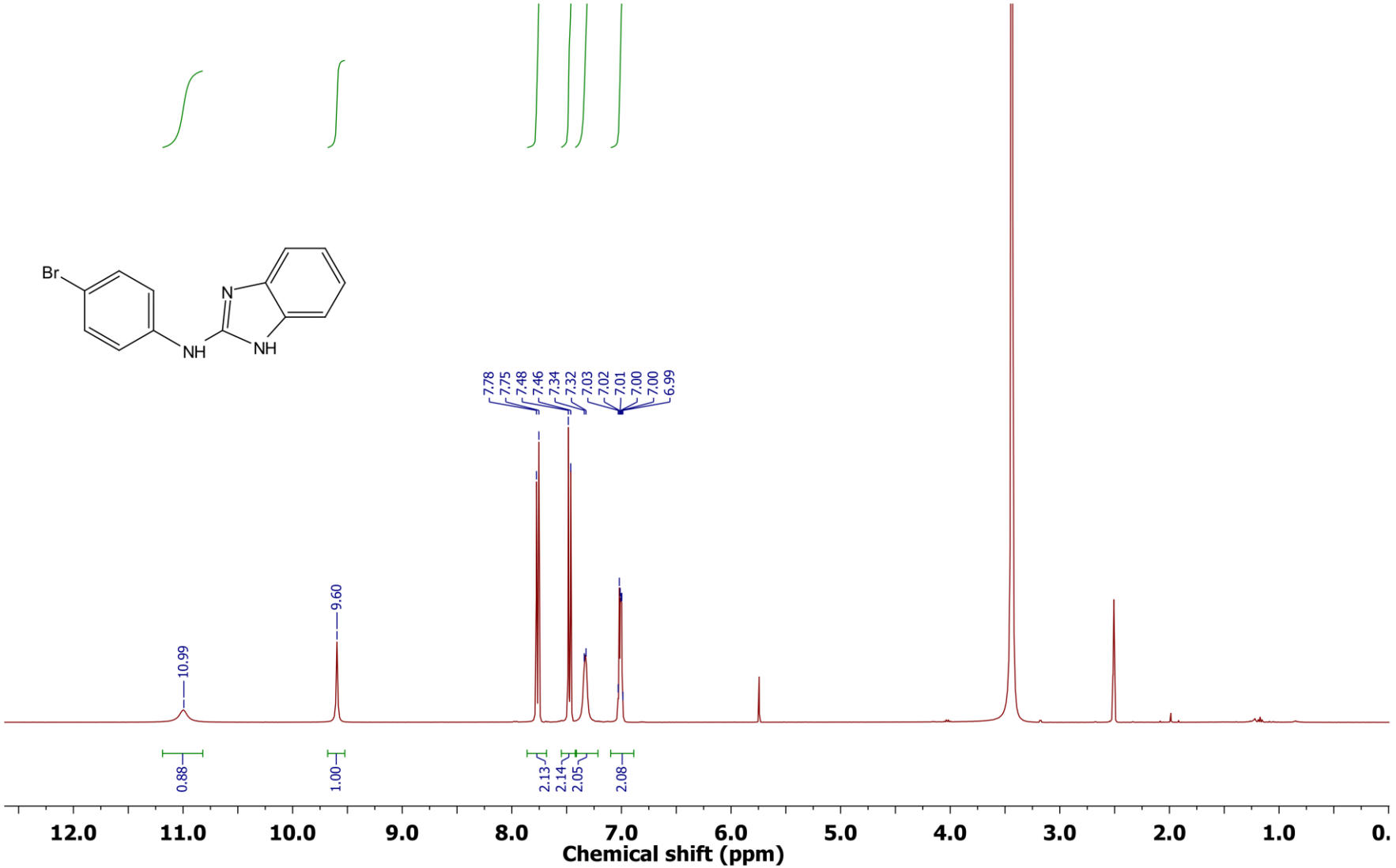

Fig. S3 ^{1}H NMR spectrum (400 MHz) of **1b** in DMSO-d_6 at room temperature.

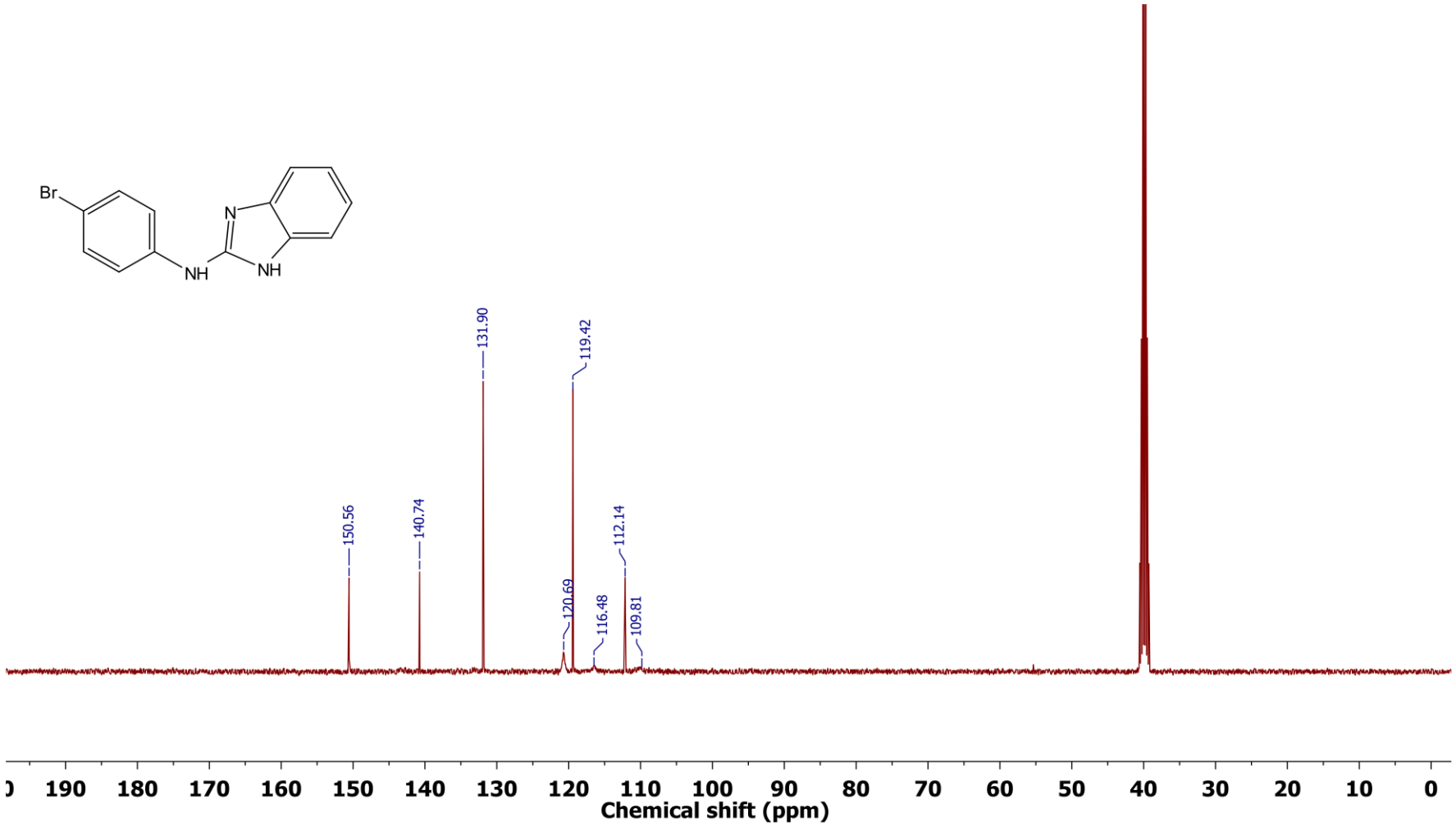

Fig. S4 ^{13}C NMR spectrum (101 MHz) of **1b** in DMSO-d_6 at room temperature.

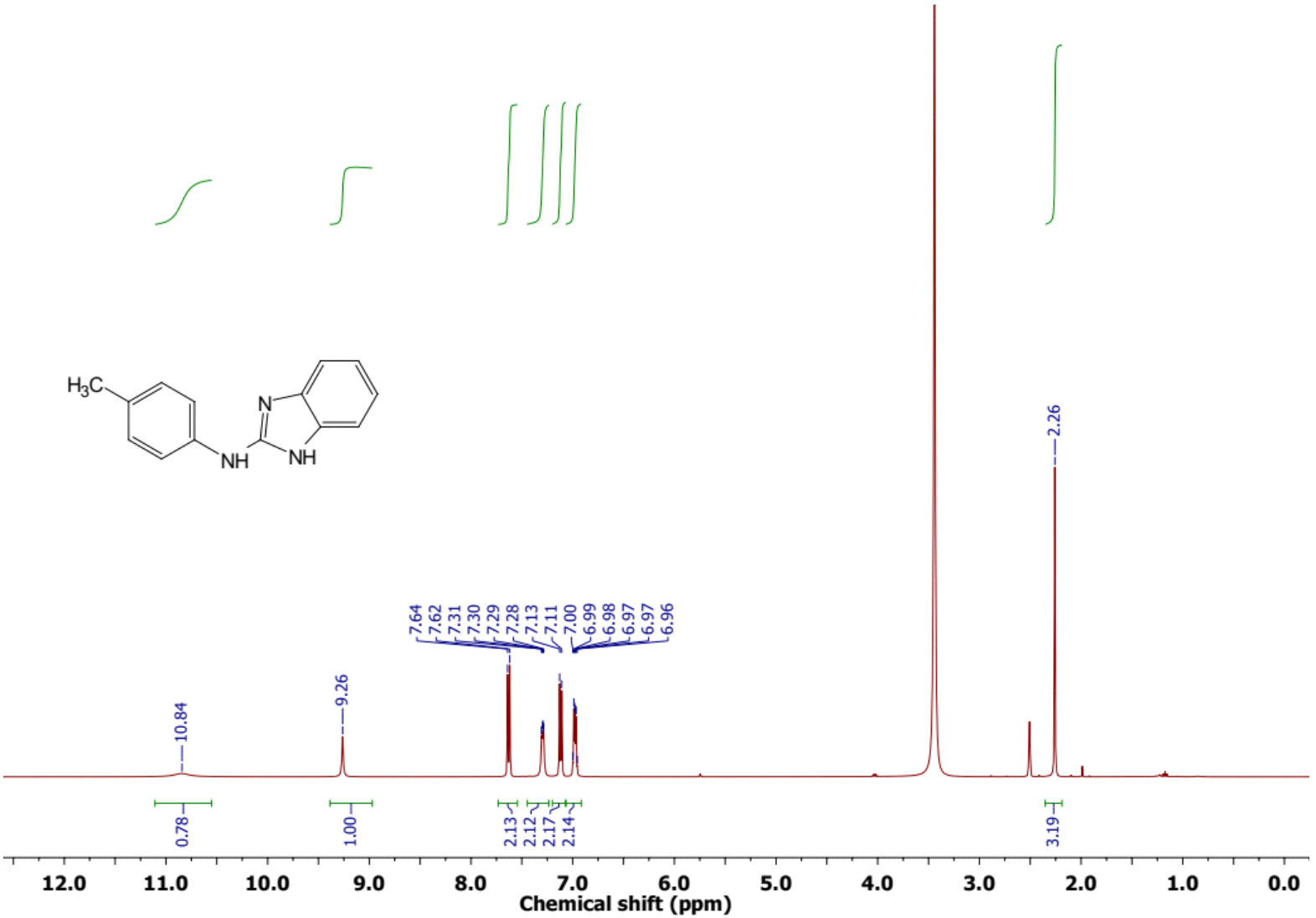

Fig. S5 ^{1}H NMR spectrum (400 MHz) of **1c** in DMSO-d_6 at room temperature.

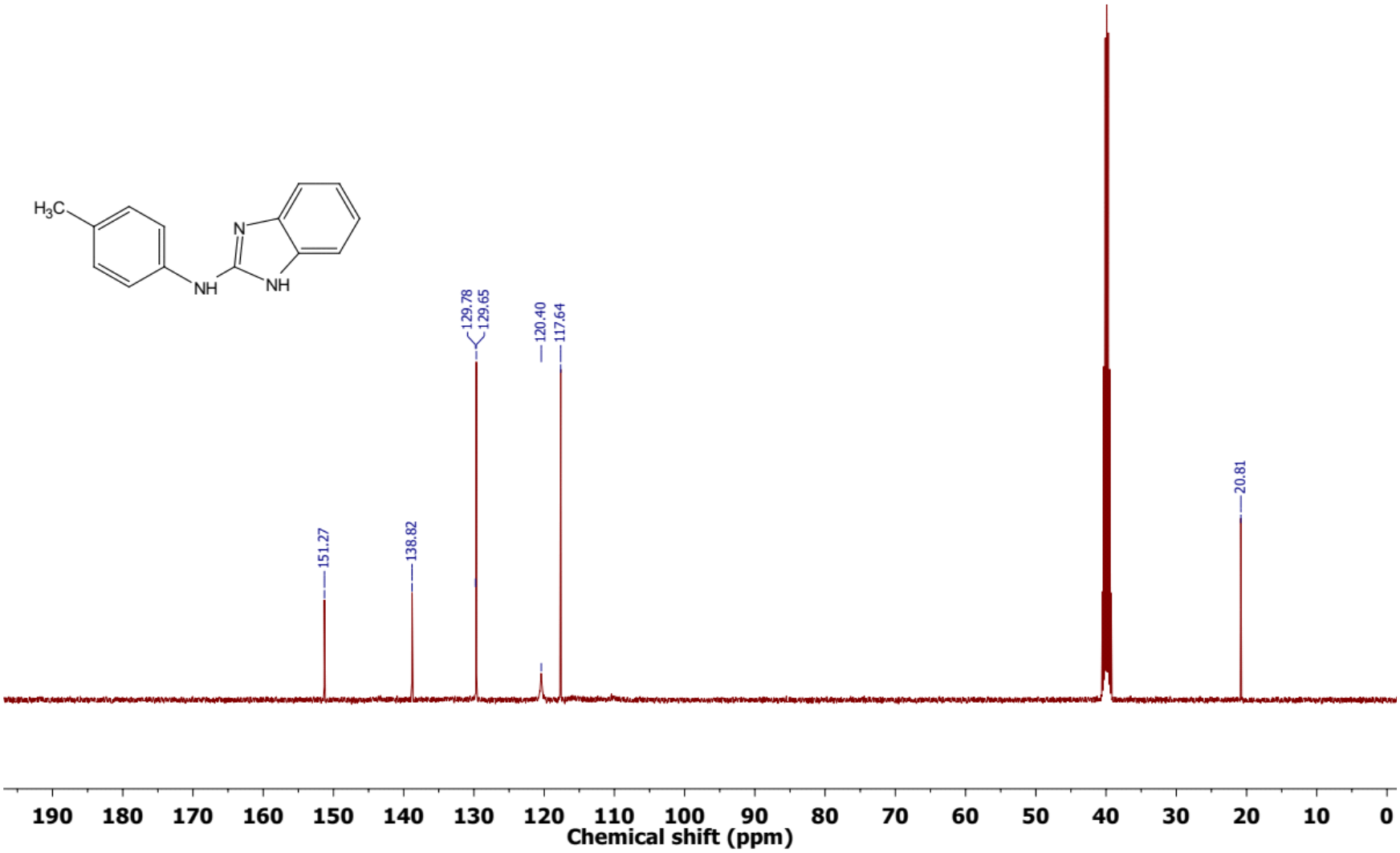

Fig. S6 ^{13}C NMR spectrum (101 MHz) of **1c** in DMSO-d_6 at room temperature.

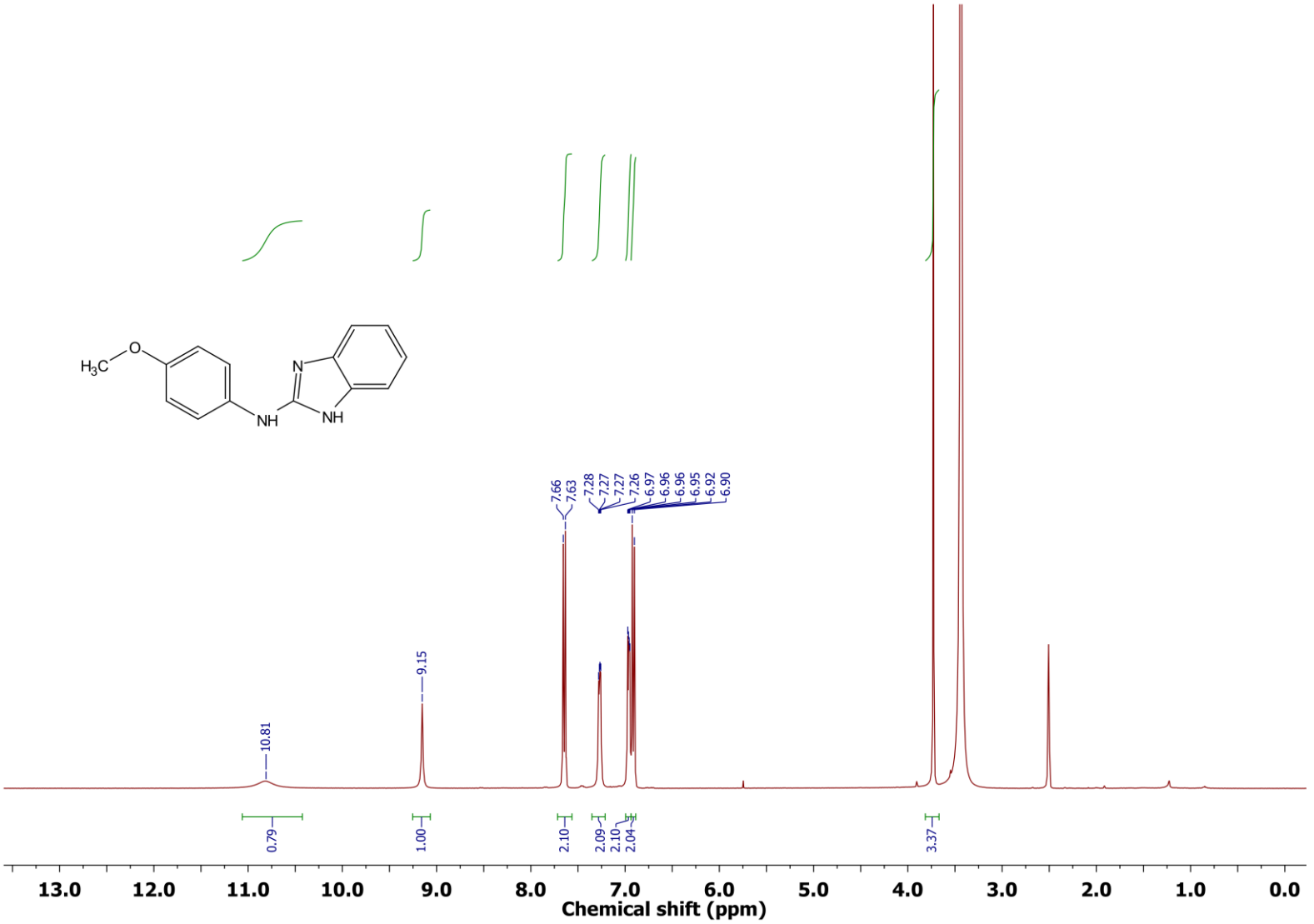

Fig. S7 ^{1}H NMR spectrum (400 MHz) of **1d** in DMSO-d_6 at room temperature.

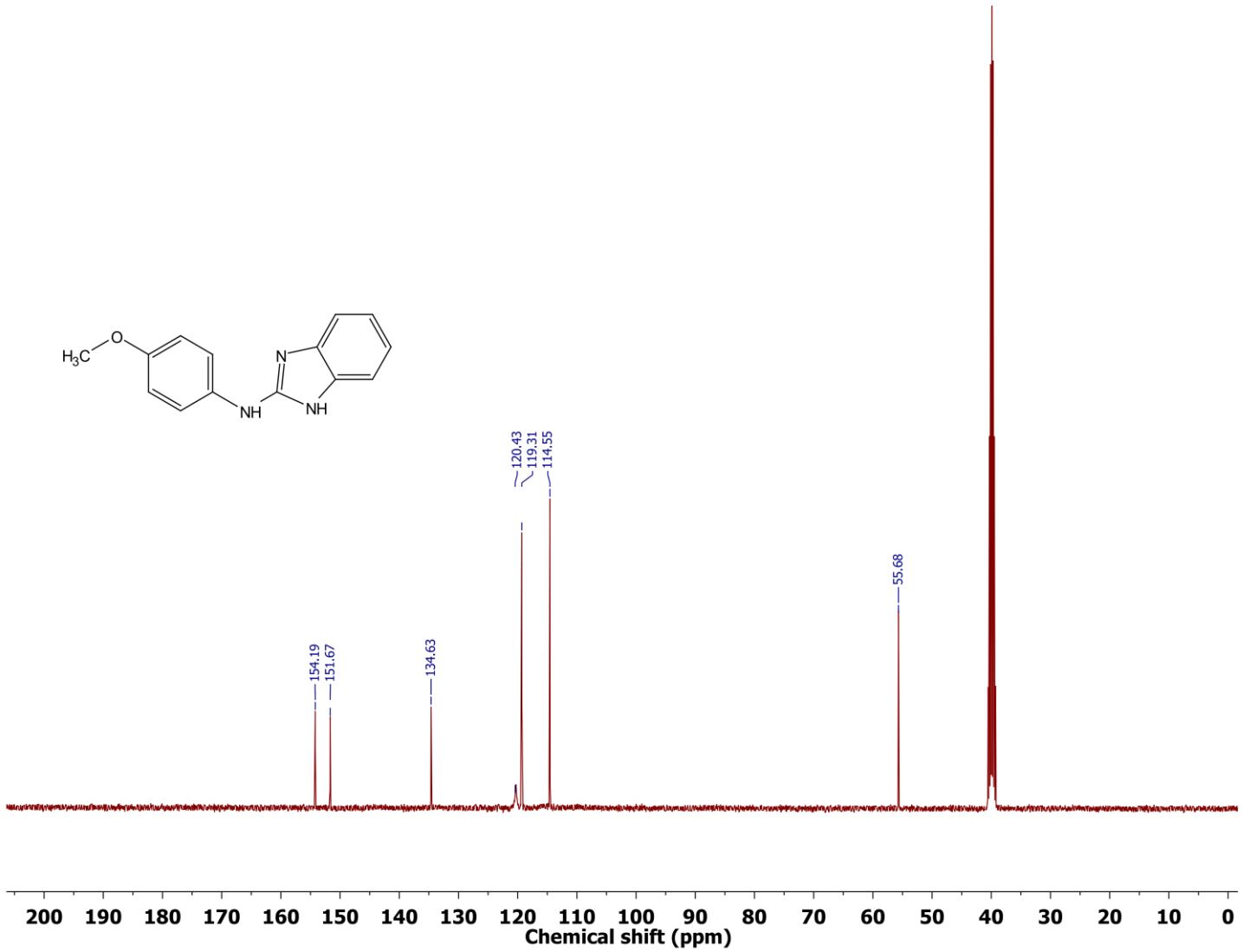

Fig. S8 ^{13}C NMR spectrum (101 MHz) of **1d** in DMSO-d_6 at room temperature.

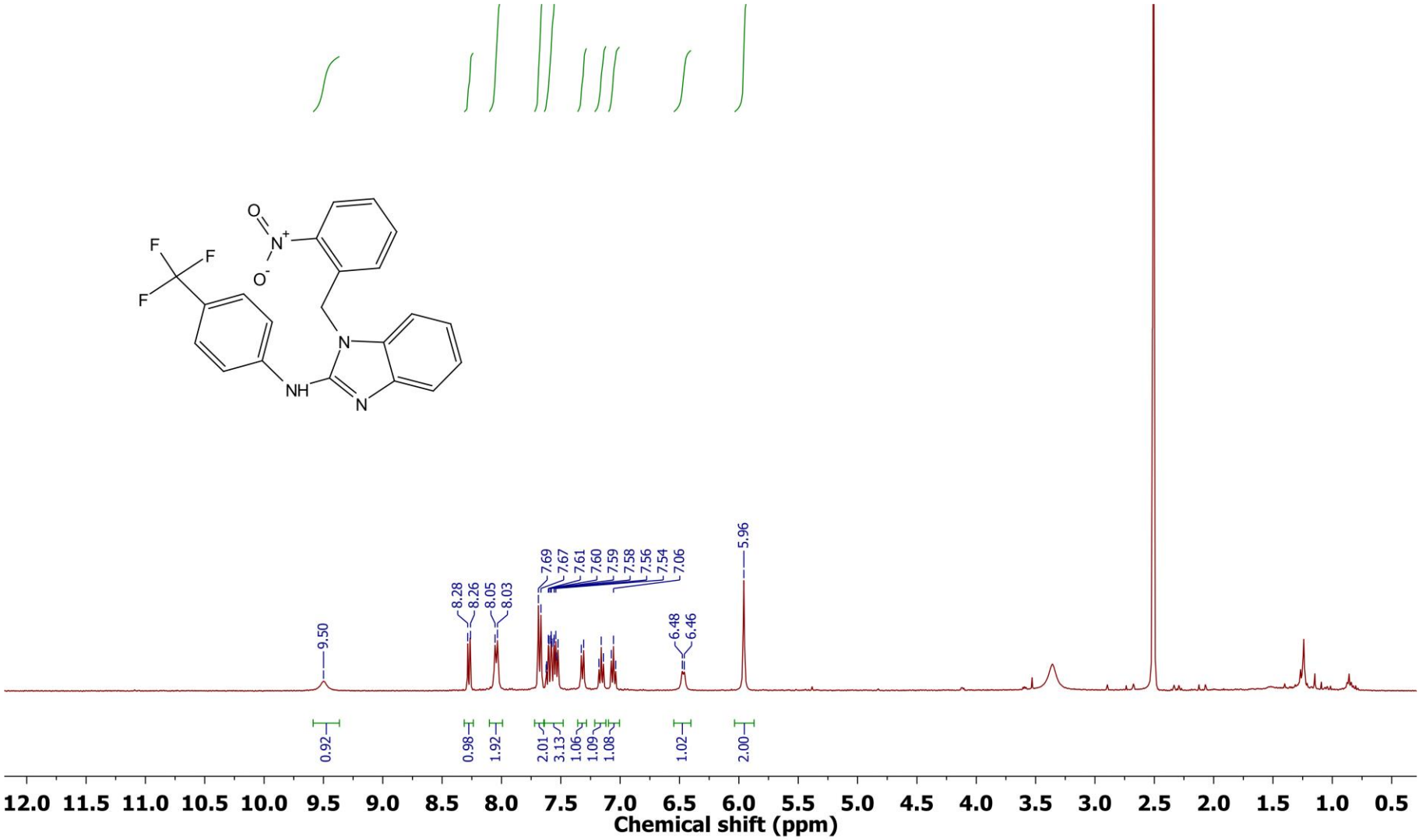

Fig. S9 ^{1}H NMR spectrum (400 MHz) of **2a** in DMSO-d_6 at room temperature.

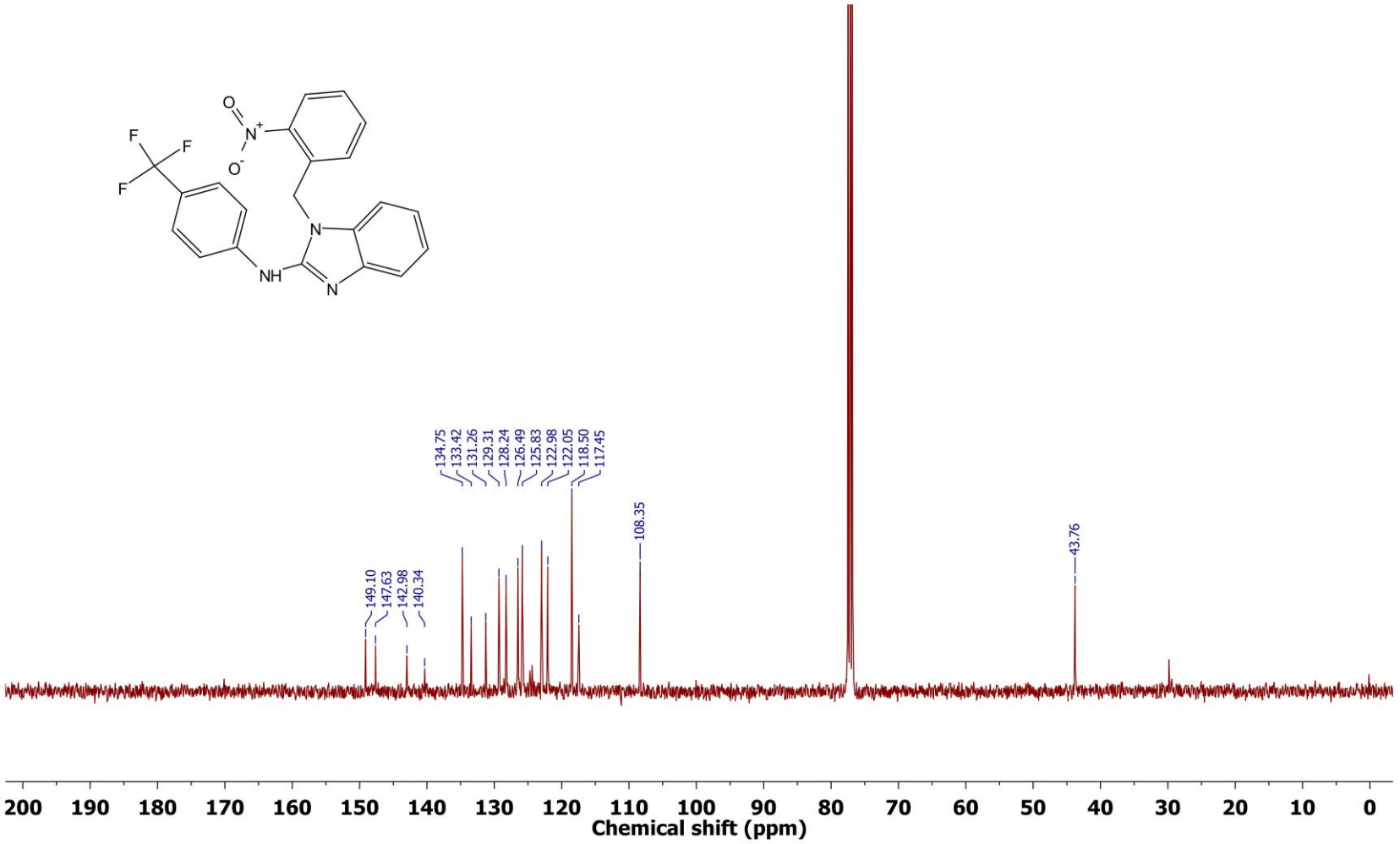

Fig. S10 ^{13}C NMR spectrum (101 MHz) of **2a** in $CDCl_3$ at room temperature.

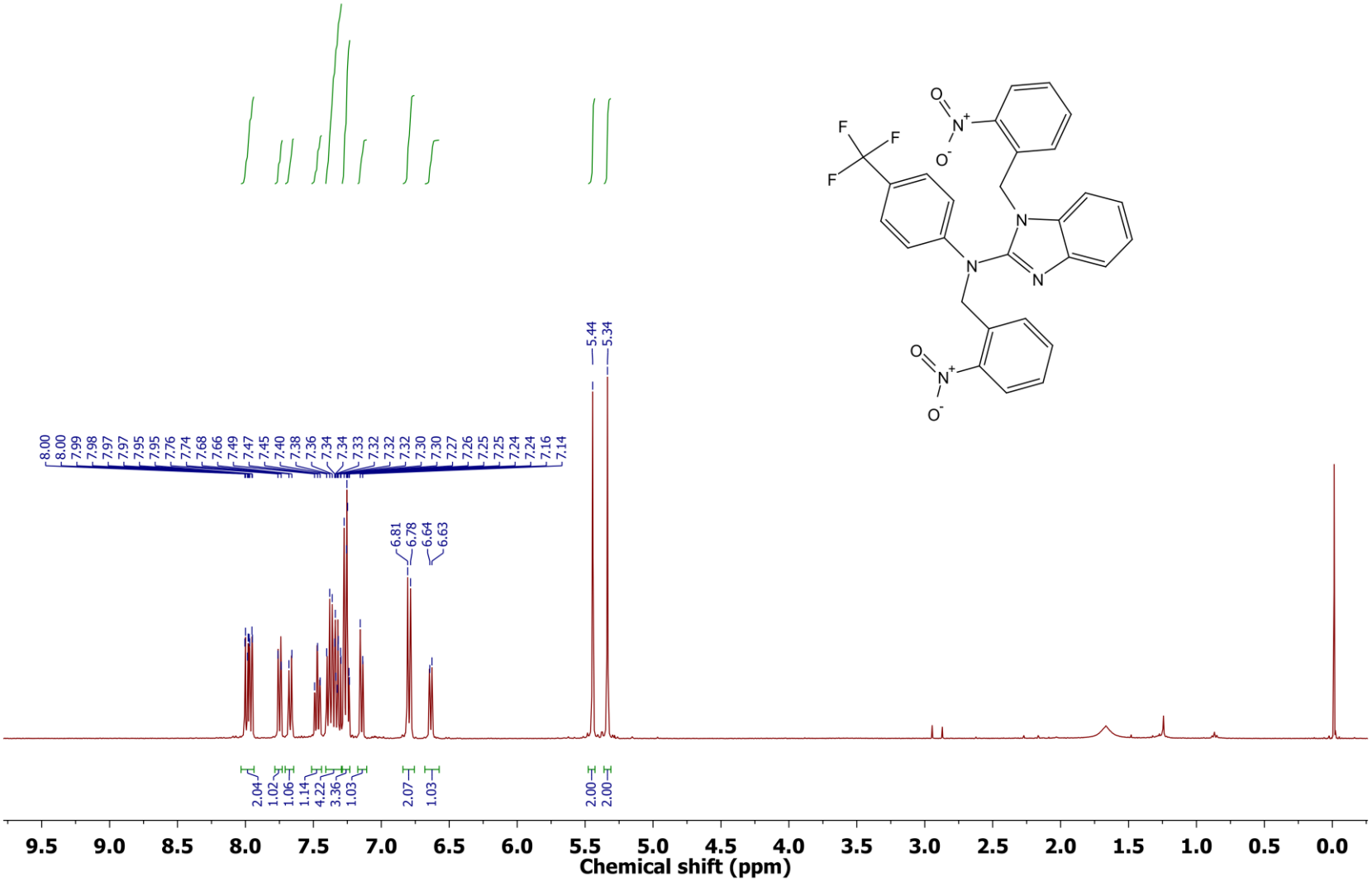

Fig. S11 ^{1}H NMR spectrum (400 MHz) of **2b** in $CDCl_3$ at room temperature.

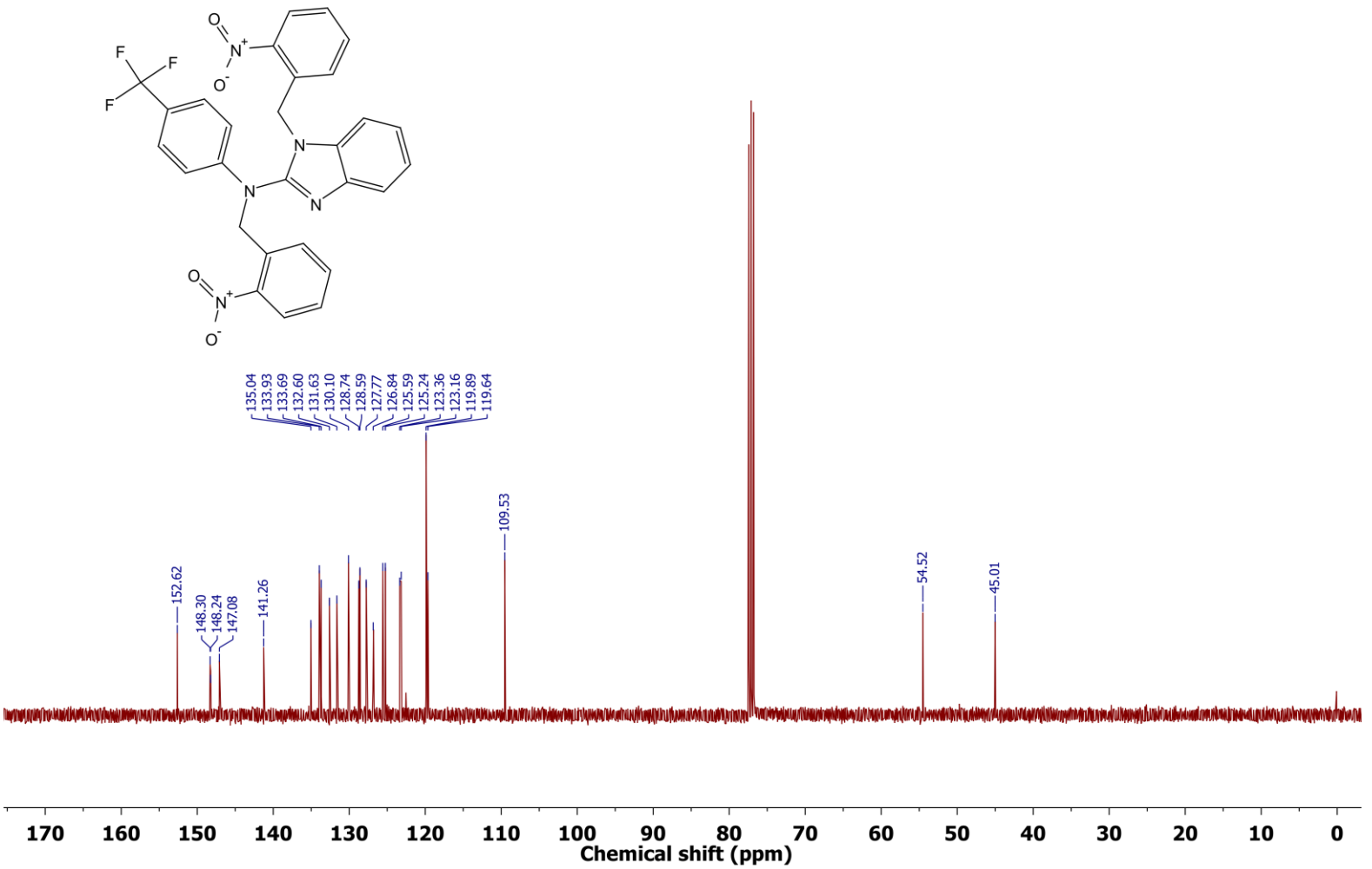

Fig. S12 ^{13}C NMR spectrum (101 MHz) of **2b** in $CDCl_3$ at room temperature.

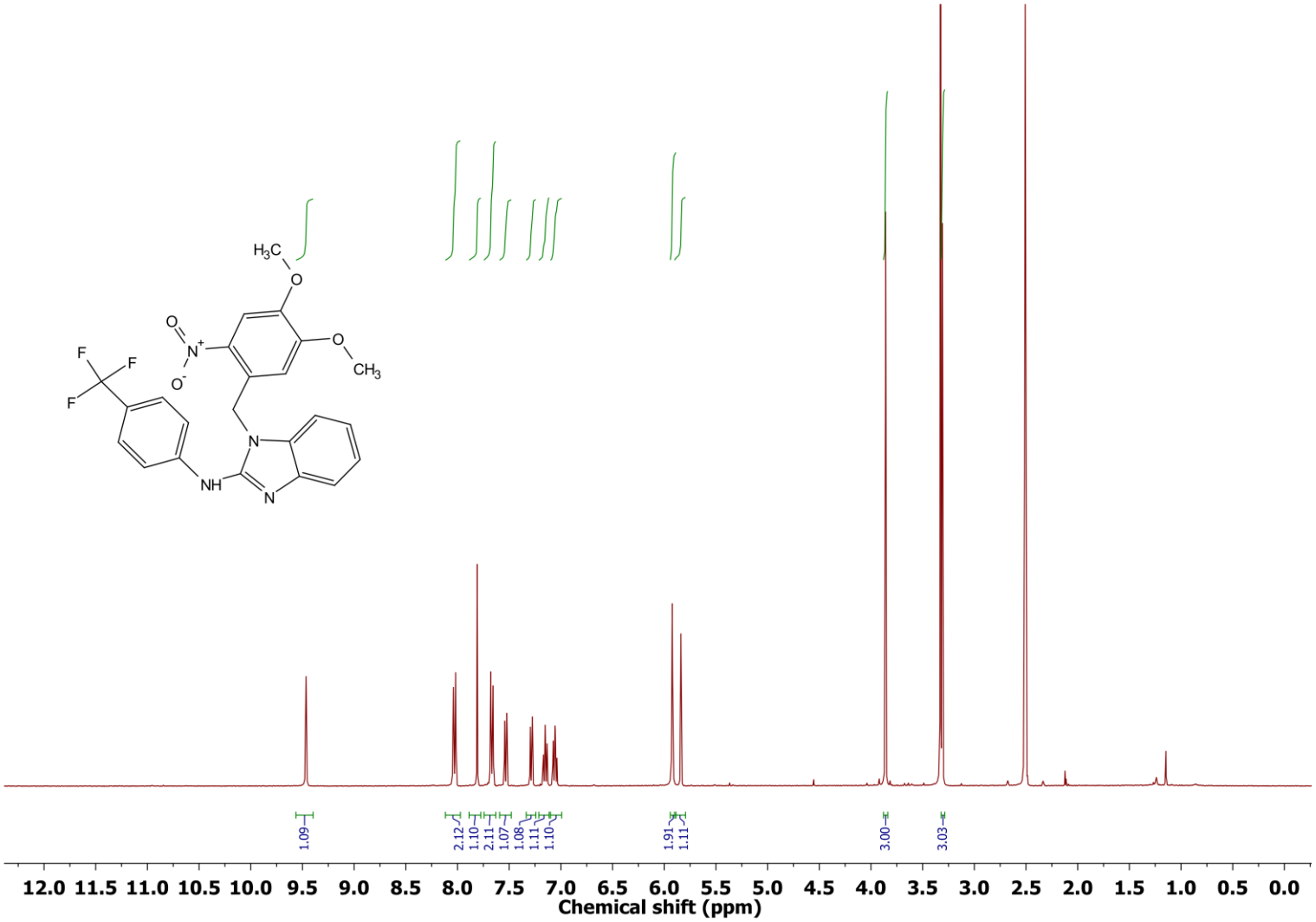

Fig. S13 ^{1}H NMR spectrum (400 MHz) of **3a** in DMSO-d_6 at room temperature.

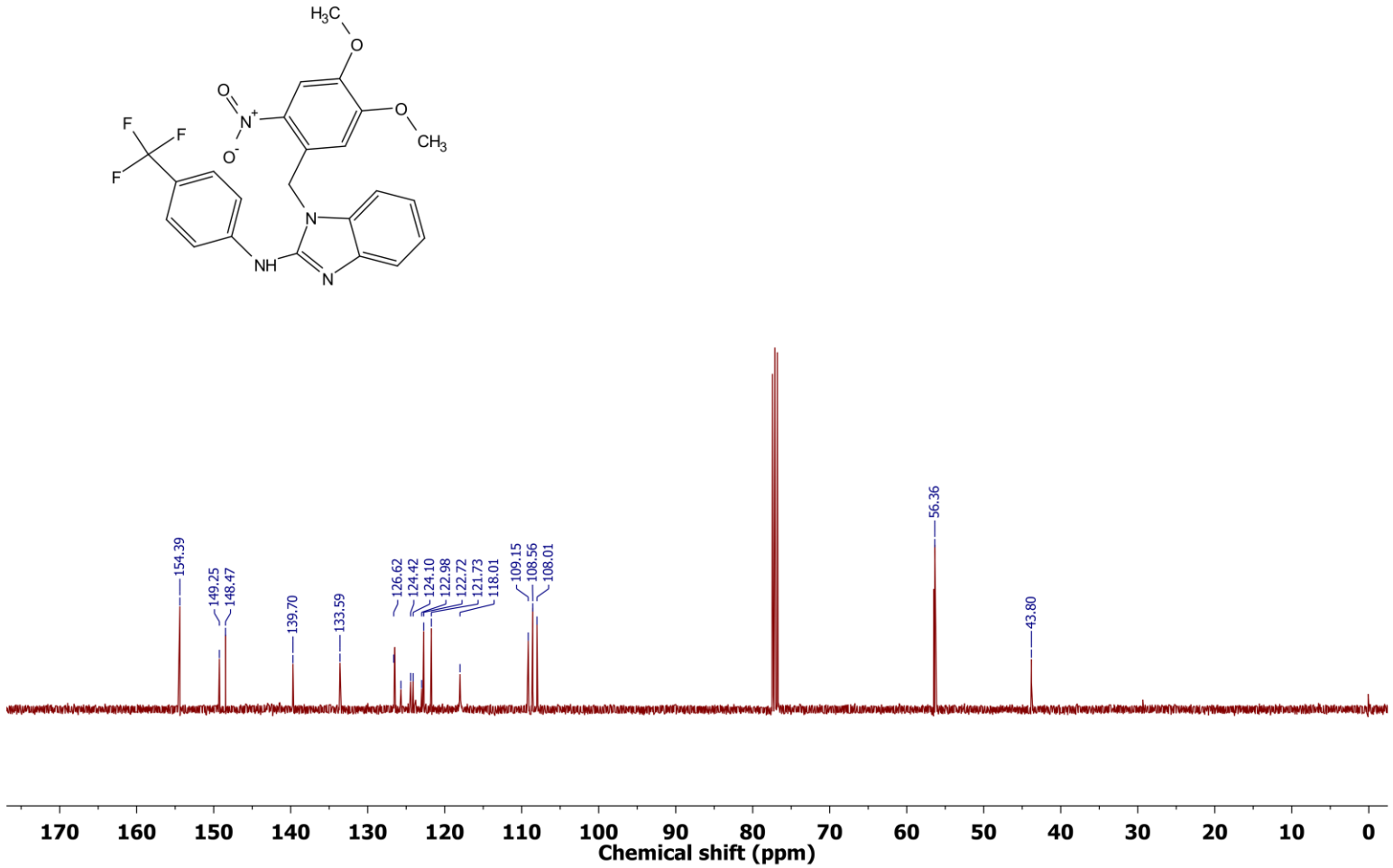

Fig. S14 ^{13}C NMR spectrum (101 MHz) of **3a** in $CDCl_3$ at room temperature.

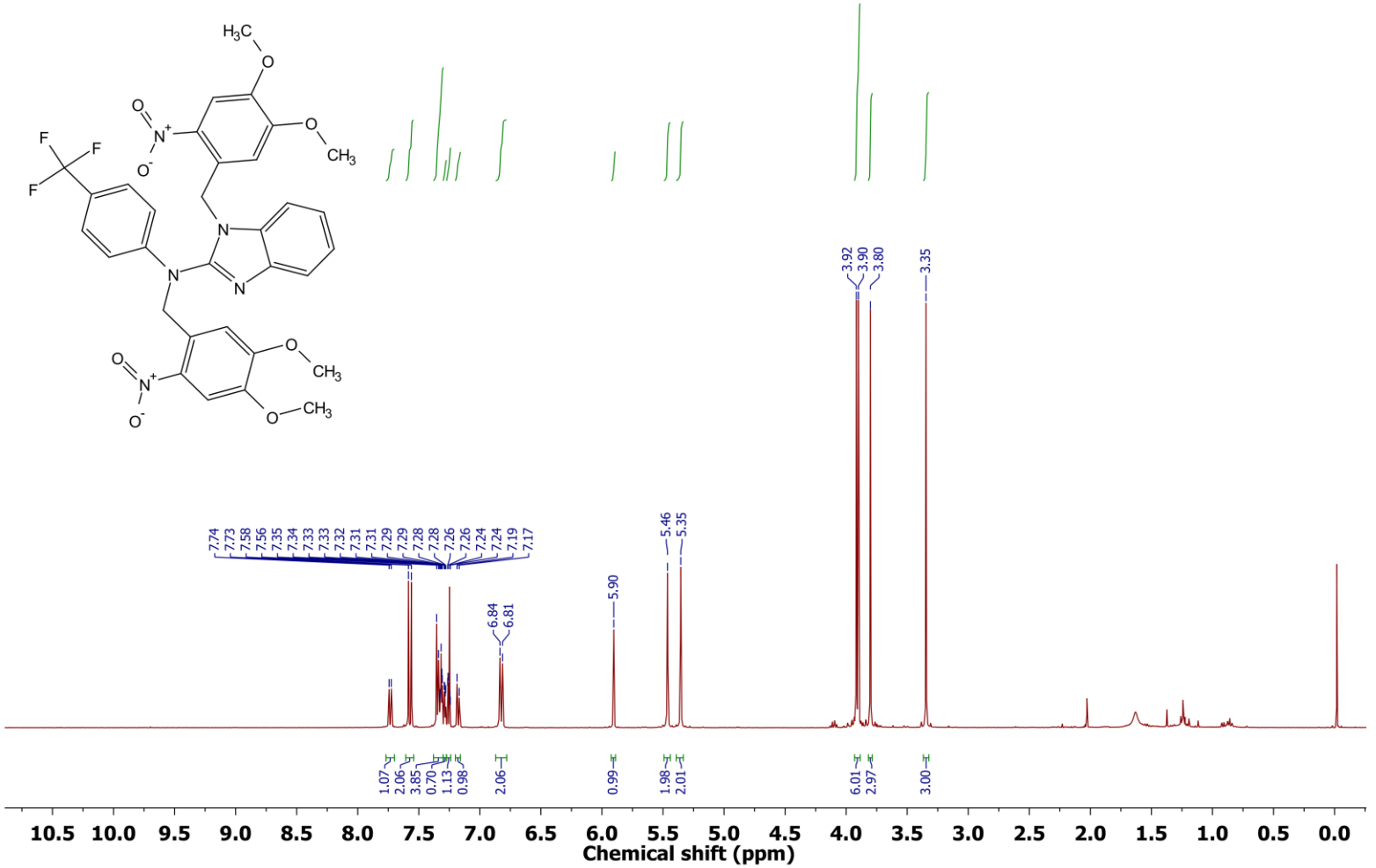

Fig. S15 ^{1}H NMR spectrum (400 MHz) of **3b** in $CDCl_3$ at room temperature.

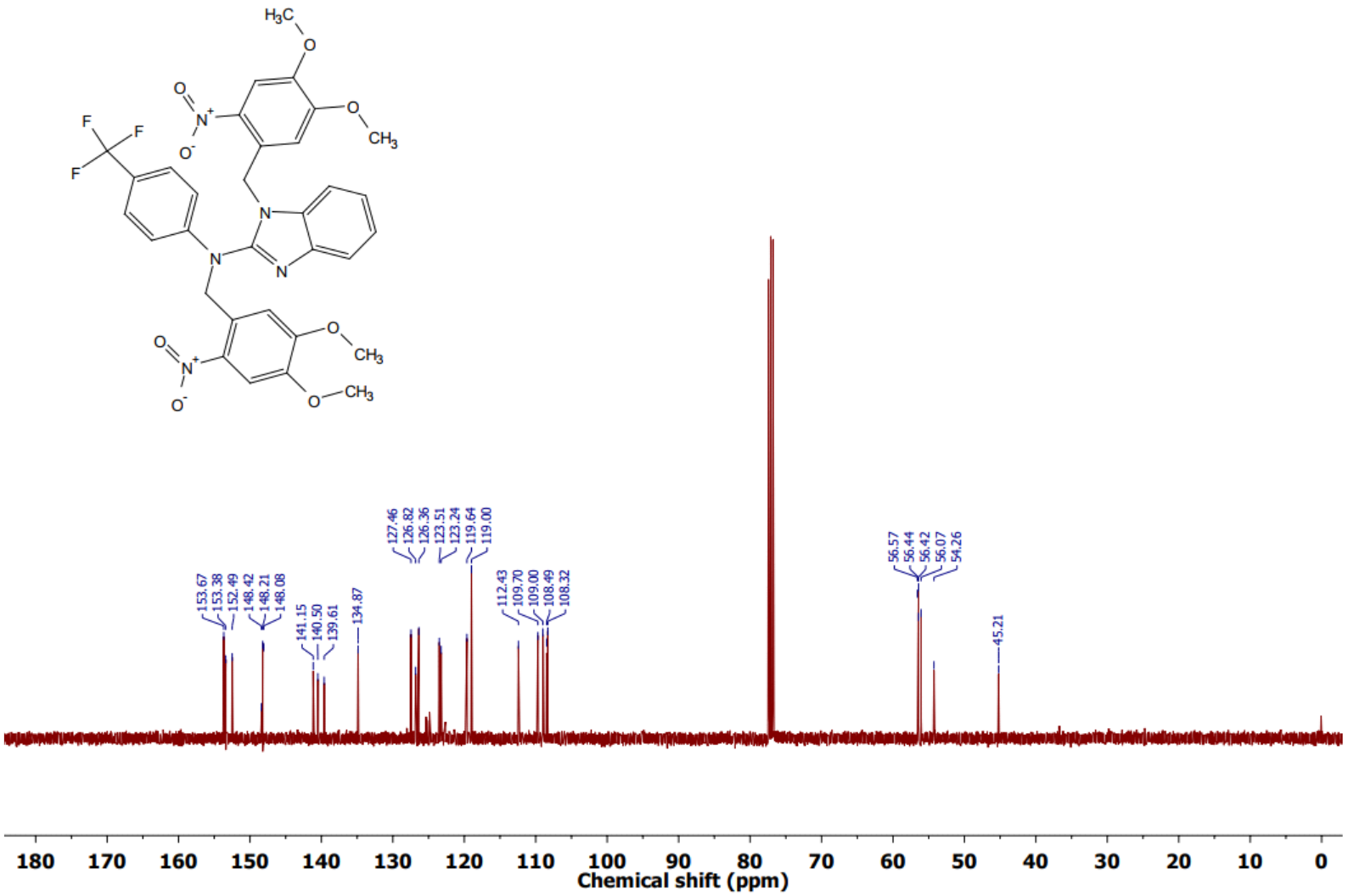

Fig. S16 ^{13}C NMR spectrum (101 MHz) of **3b** in $CDCl_3$ at room temperature.

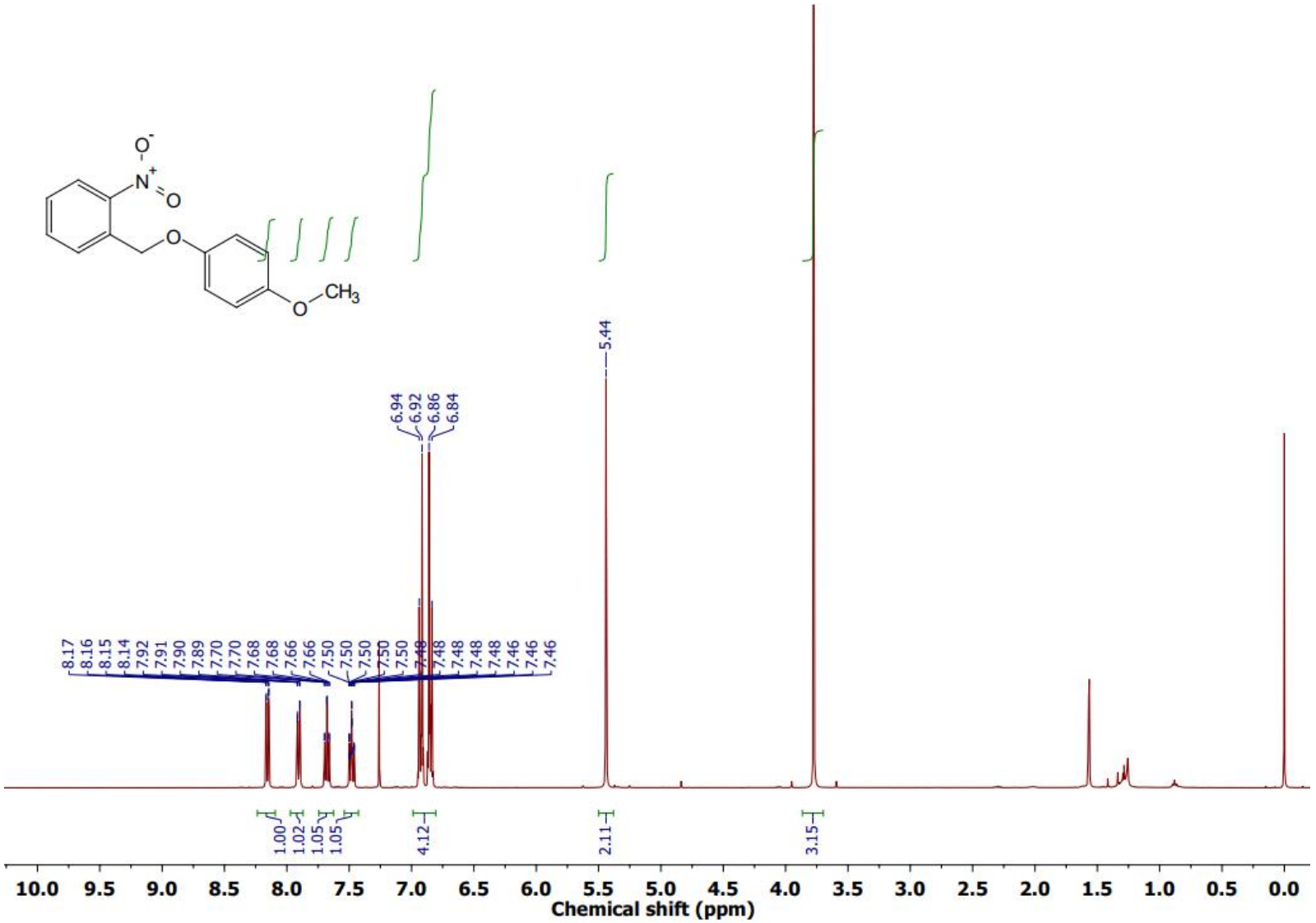

Fig. S17 ^{1}H NMR spectrum (400 MHz) of **9a** in $CDCl_3$ at room temperature.

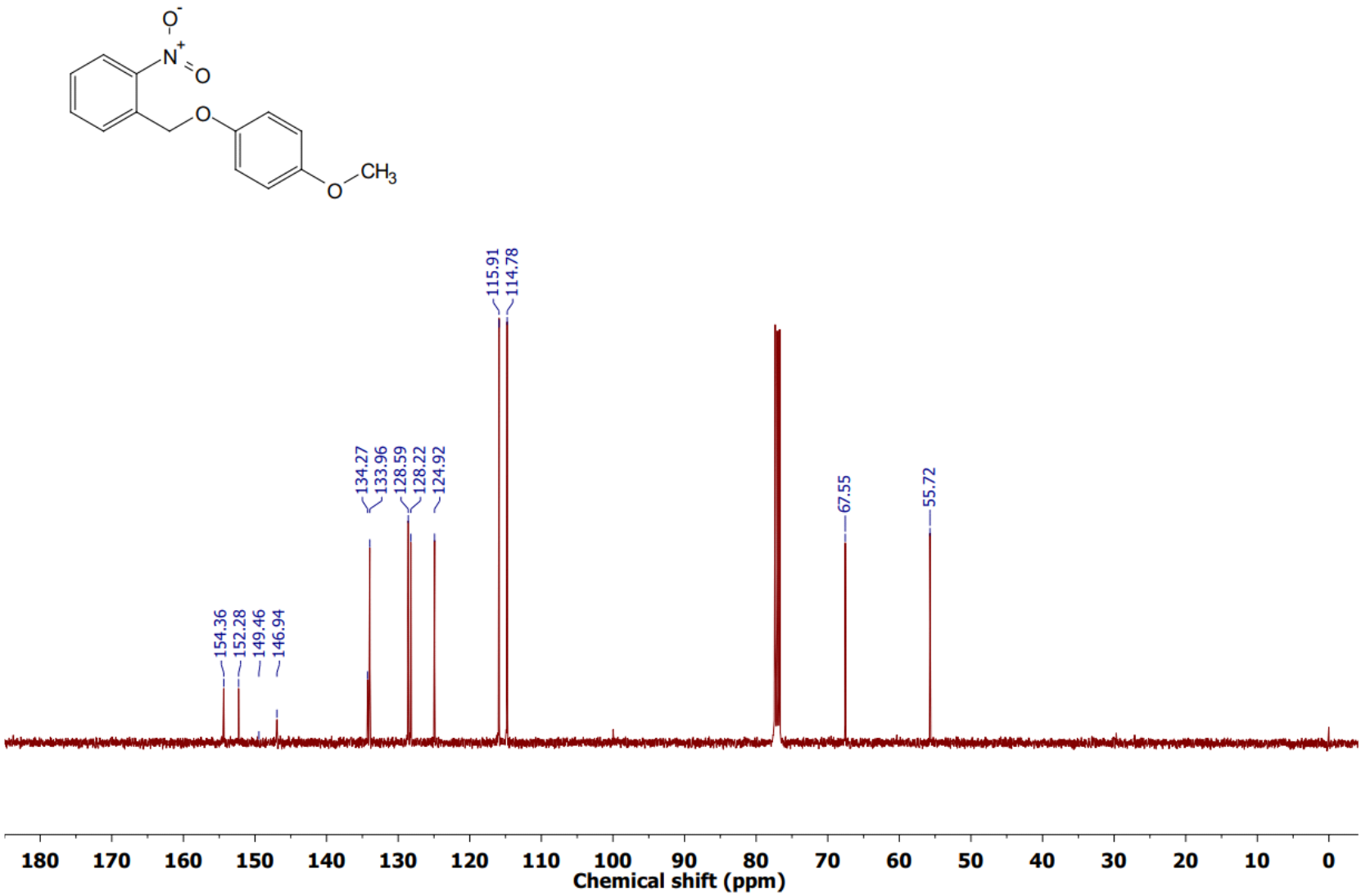

Fig. S18 ^{13}C NMR spectrum (101 MHz) of **9a** in $CDCl_3$ at room temperature.

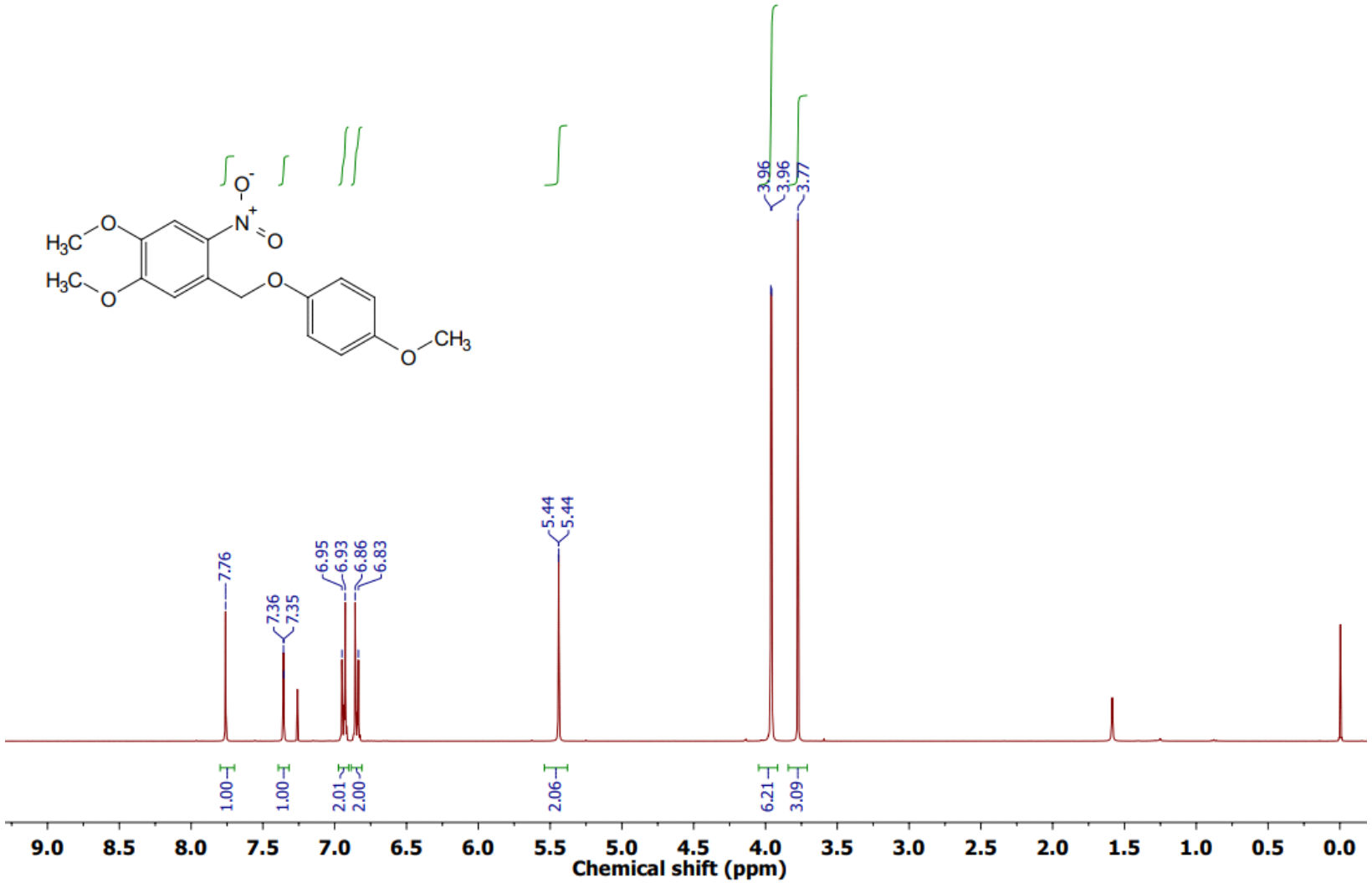

Fig. S19 ^{1}H NMR spectrum (400 MHz) of **9b** in $CDCl_3$ at room temperature.

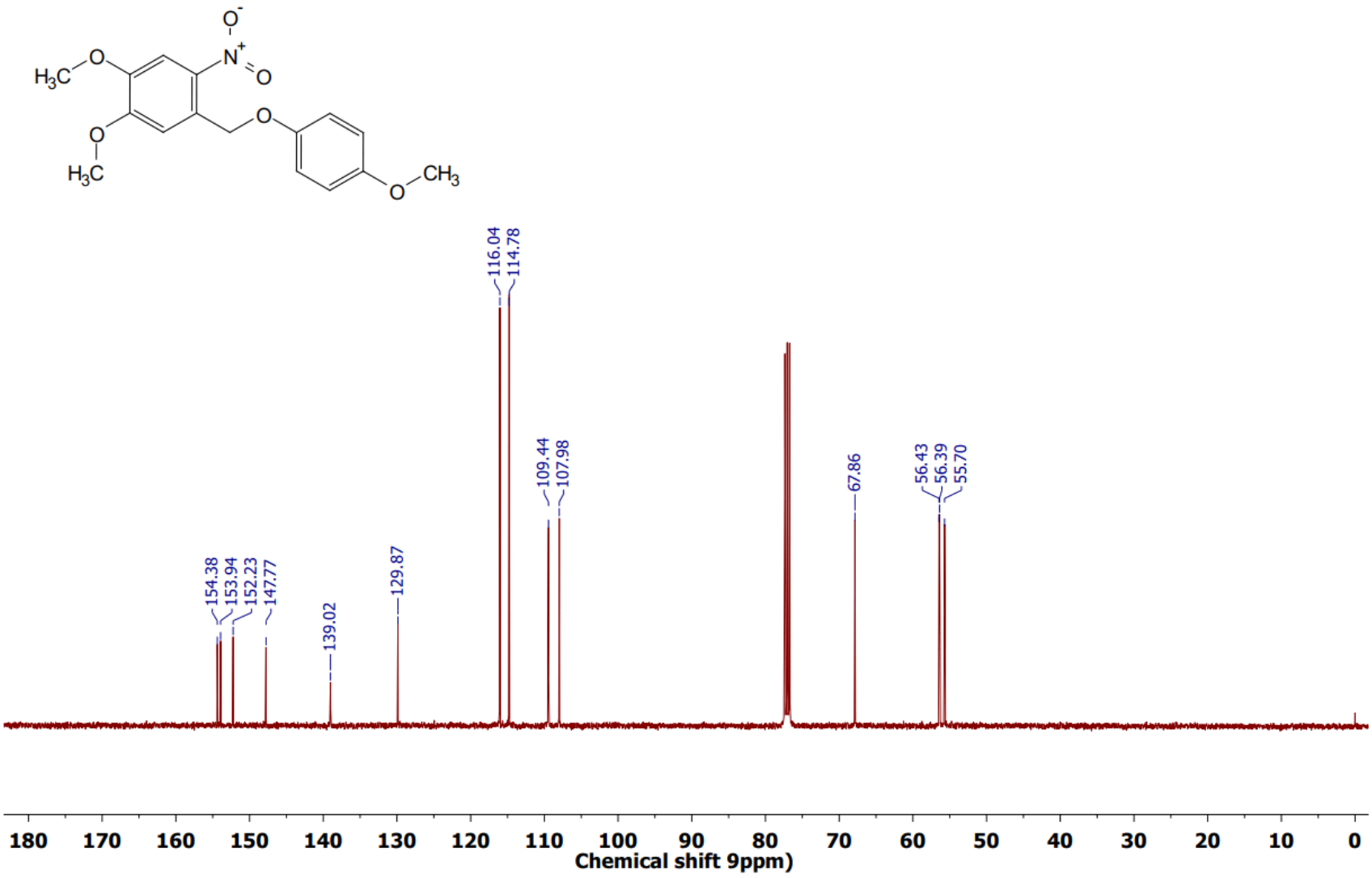

Fig. S20 ^{13}C NMR spectrum (101 MHz) of **9b** in $CDCl_3$ at room temperature.

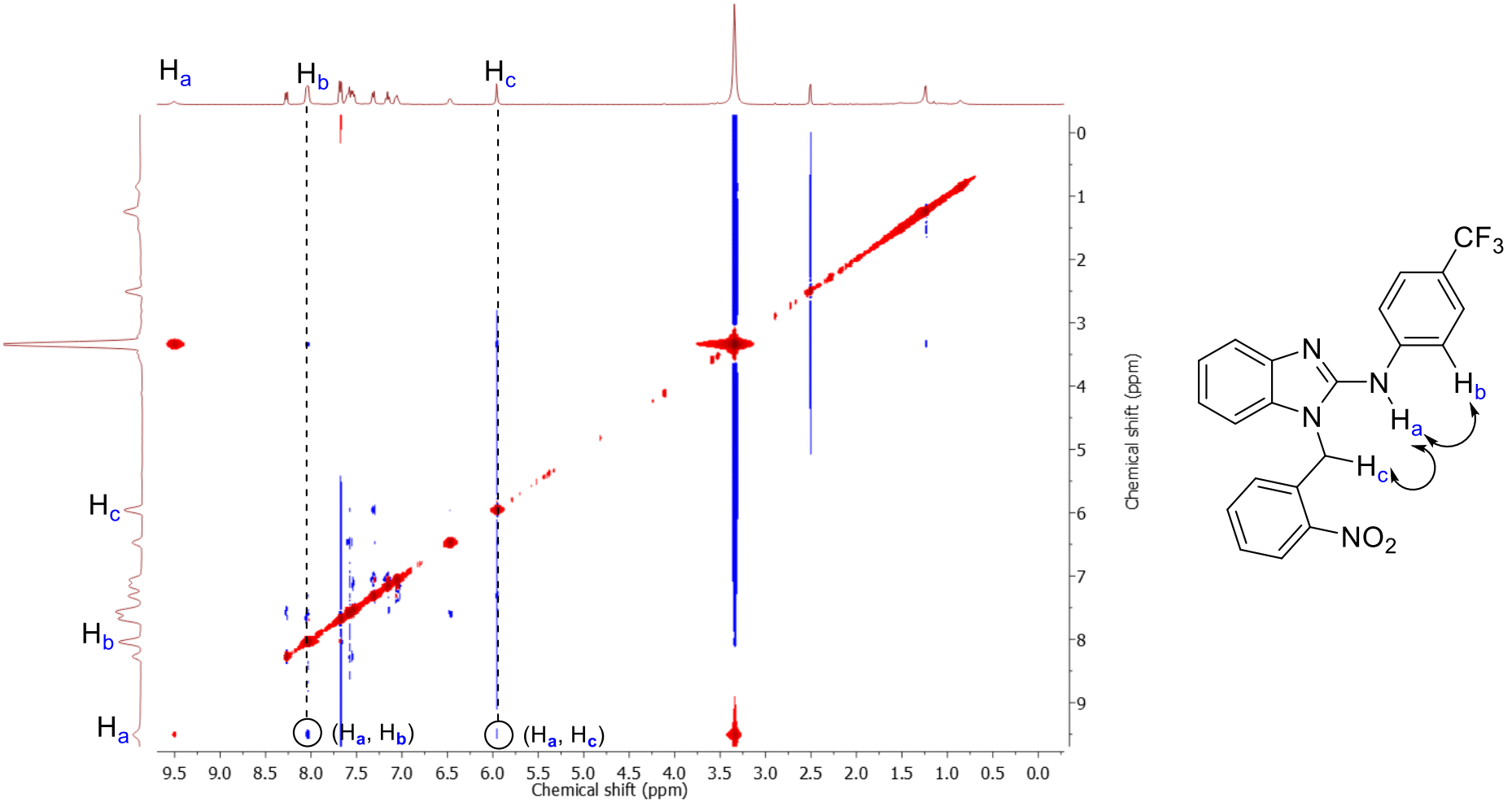

Fig. S21 ^{1}H-^{1}H NOESY spectrum (400 MHz) of **2a** in DMSO-d_6 at room temperature.

V. Anion binding studies by ^{1}H NMR spectroscopy.

^{1}H NMR titration was carried out at room temperature on a Bruker 400 MHz spectrometer. The residual solvent signal (CD_3CN, δ_H = 1.94) was considered as an internal reference to calibrate spectra. The TBACl salt and receptors were dried in a high vacuum before use. The titrations were performed by the addition of aliquots from TBACl solution (0.25 M in CD_3CN) to the solution of either **1a**, **1b**, **1c**, or **1d**, (0.0025 M in CD_3CN). All NMR data were processed using MestreNova 6.0 and collected data were fitted in different binding modes using BindFit.[S1, S2]

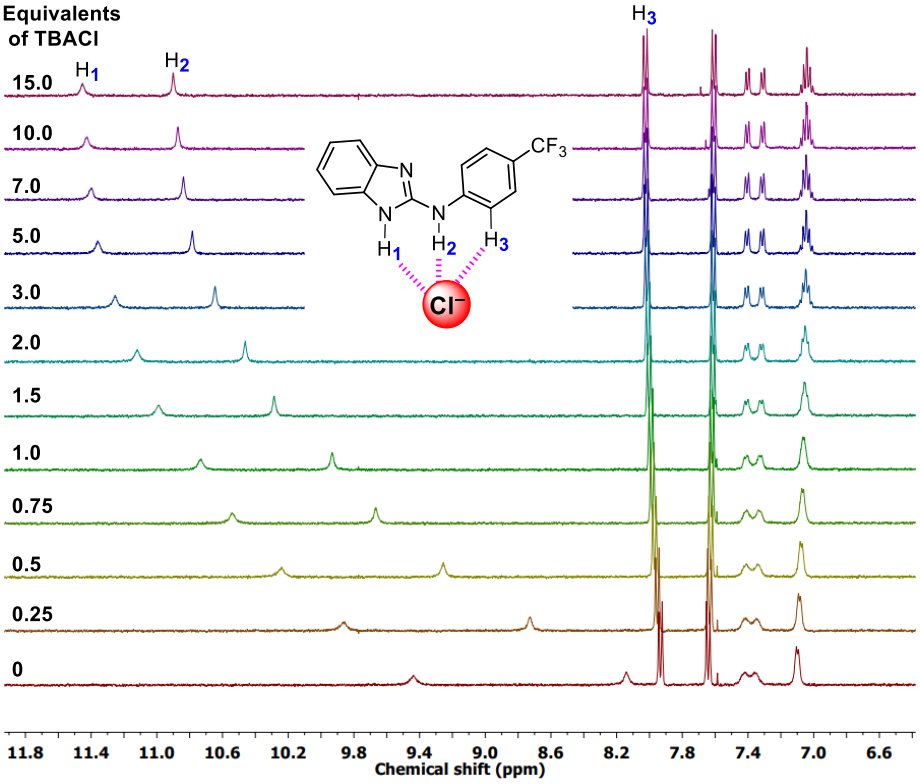

Fig. S22 ^{1}H NMR titration spectra for **1a** (2.5 mM) with stepwise addition of TBACl in CD_3CN. The equivalents of added TBACl are shown on the stacked spectra.

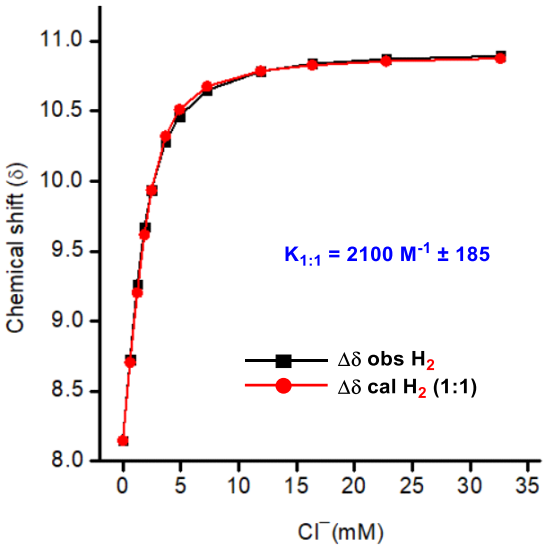

Fig. S23 The plot of chemical shift (δ) of H_2 protons *vs* concentration of TBACl added, fitted to 1:1 binding model of BindFit v0.5. The binding constant obtained is the mean of the three independent experiments.

http://app.supramolecular.org/bindfit/view/3e5f0864-e3bf-40f6-9d88-6dd24d8ba47a-(**1a** with Cl^-).

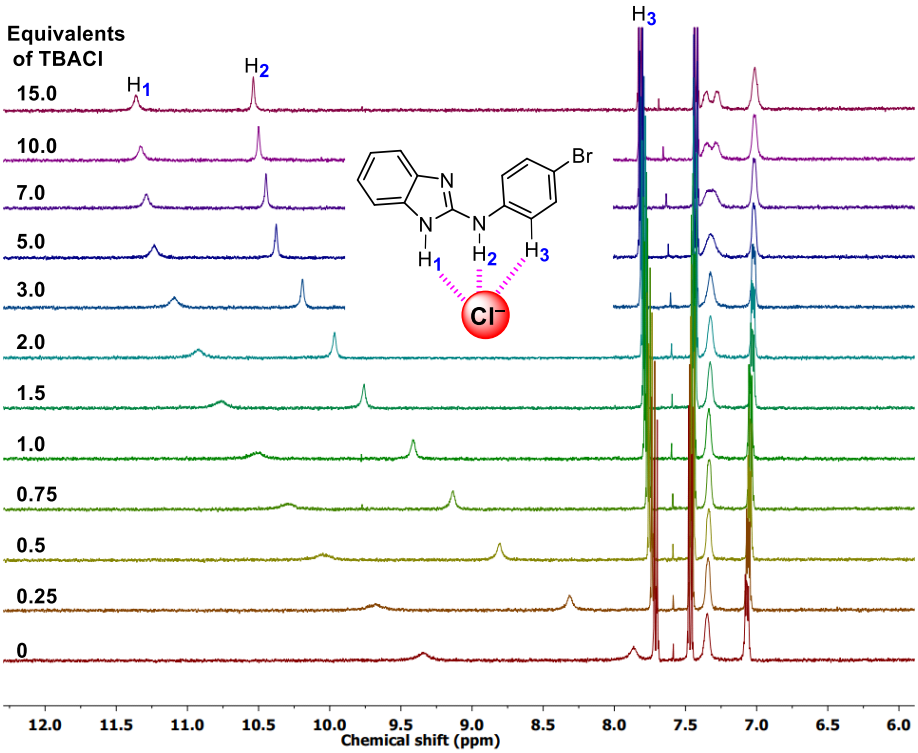

Fig. S24 ^1H NMR titration spectra for **1b** (2.5 mM) with stepwise addition of TBACl in CD_3CN. The equivalents of added TBACl are shown on the stacked spectra.

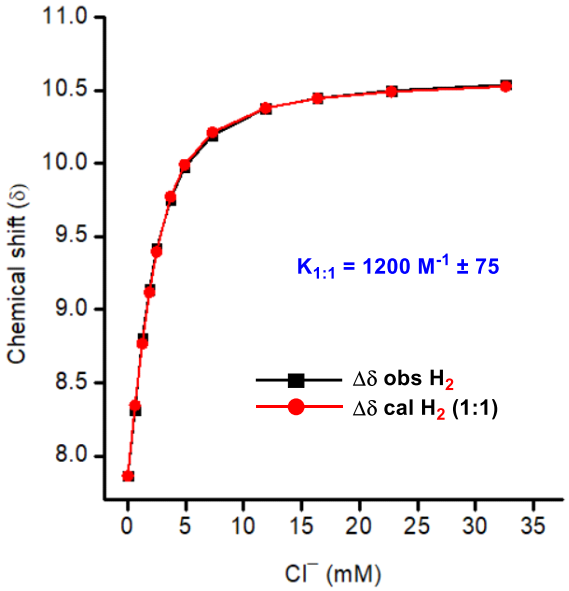

Fig. S25 The plot of chemical shift (δ) of H_2 protons *vs* concentration of TBACl added, fitted to 1:1 binding model of BindFit v0.5. The binding constant obtained is the mean of the three independent experiments.

http://app.supramolecular.org/bindfit/view/ca1c659c-633d-4b2c-9813-a19b9a164fed-(**1b** with Cl^-).

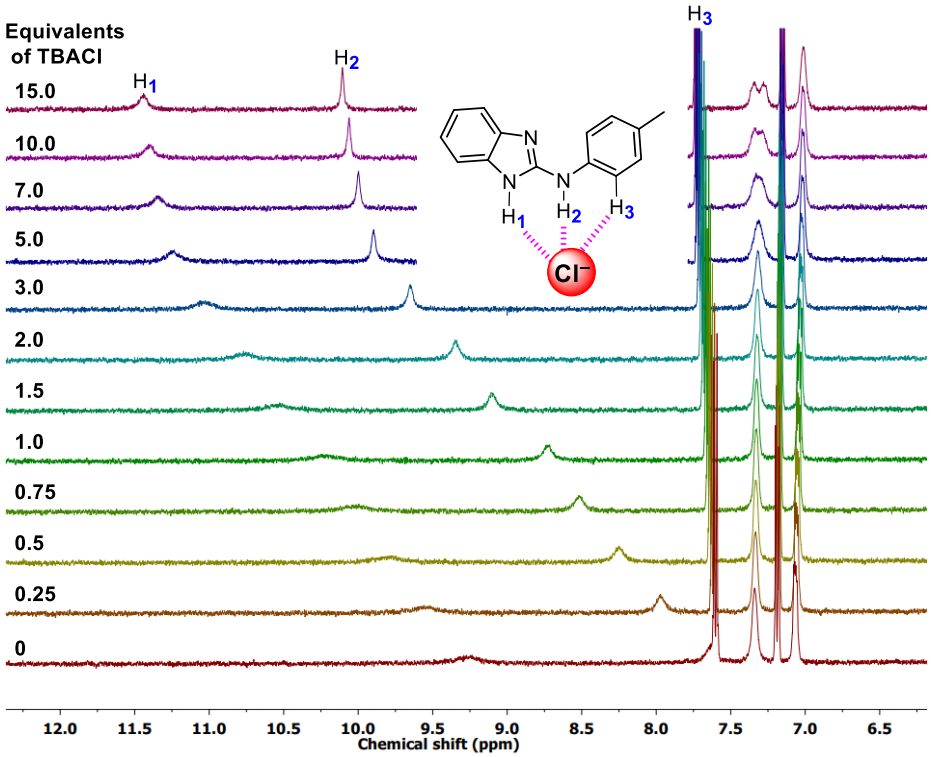

Fig. S26 ^1H NMR titration spectra for **1c** (2.5 mM) with stepwise addition of TBACl in CD_3CN. The equivalents of added TBACl are shown on the stacked spectra.

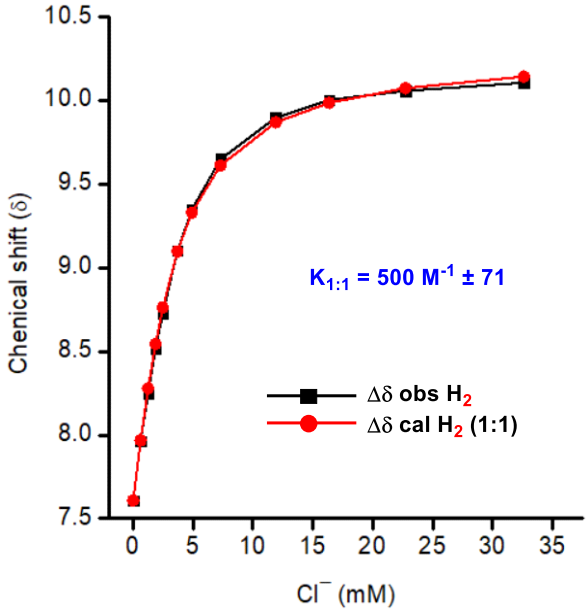

Fig. S27 The plot of chemical shift (δ) of H_2 protons *vs* concentration of TBACl added, fitted to 1:1 binding model of BindFit v0.5. The binding constant obtained is the mean of the three independent experiments.

http://app.supramolecular.org/bindfit/view/5c21c67a-cdfa-4a43-942d-5d10ee04d422-(**1c** with Cl^-).

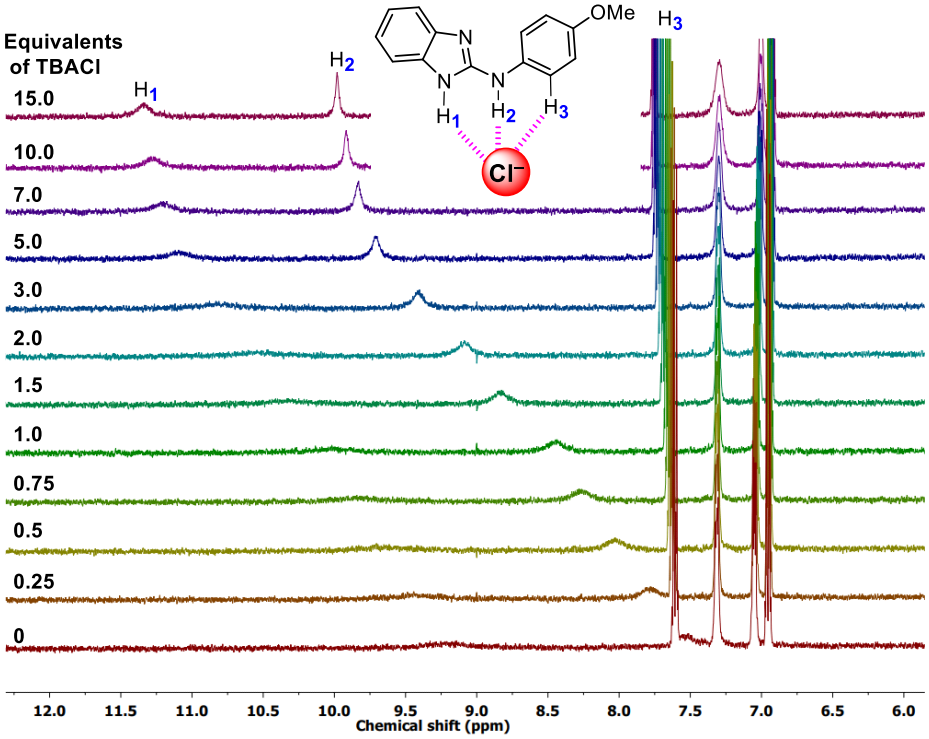

Fig. S28 ^{1}H NMR titration spectra for **1d** (2.5 mM) with stepwise addition of TBACl in CD_3CN. The equivalents of added TBACl are shown on the stacked spectra.

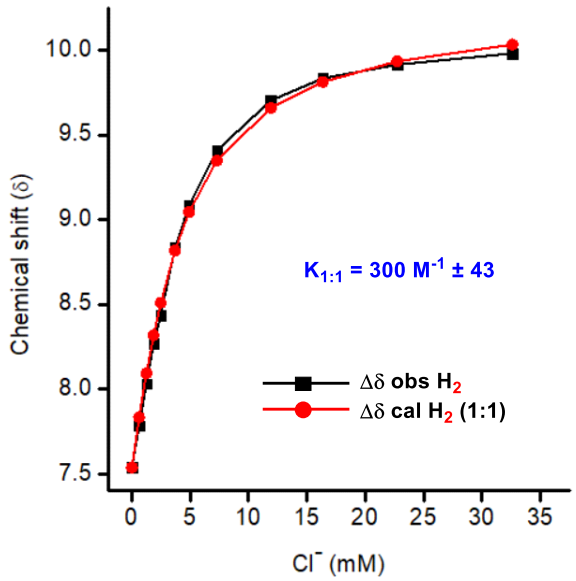

Fig. S29 The plot of chemical shift (δ) of H_2 protons *vs* concentration of TBACl added, fitted to 1:1 binding model of BindFit v0.5. The binding constant obtained is the mean of the three independent experiments.

http://app.supramolecular.org/bindfit/view/bb20b05f-8f45-411c-b7ea-723335544f75-(**1d** with Cl^-).

VI. Mass spectrometric studies.

Compound **1a** and TMACl (Tetramethylammonium chloride) (1 mM each) were mixed in the ratio of **1a:**TMACl (1:1) in CH_3CN. The solution was electro sprayed at a flow rate of 5.0 μL/min. A constant spray and highest intensities were achieved with a capillary voltage of 2500 V at a source temperature of 80 °C. The parameters for sample cone (20 V) and extractor cone voltage (5 V) were optimized for maximum intensities of the desired complexes. Fig. S30 represents the ESI-MS data recorded from CH_3CN solution of **1a** with TMACl prepared in 1:1 molar ratio.

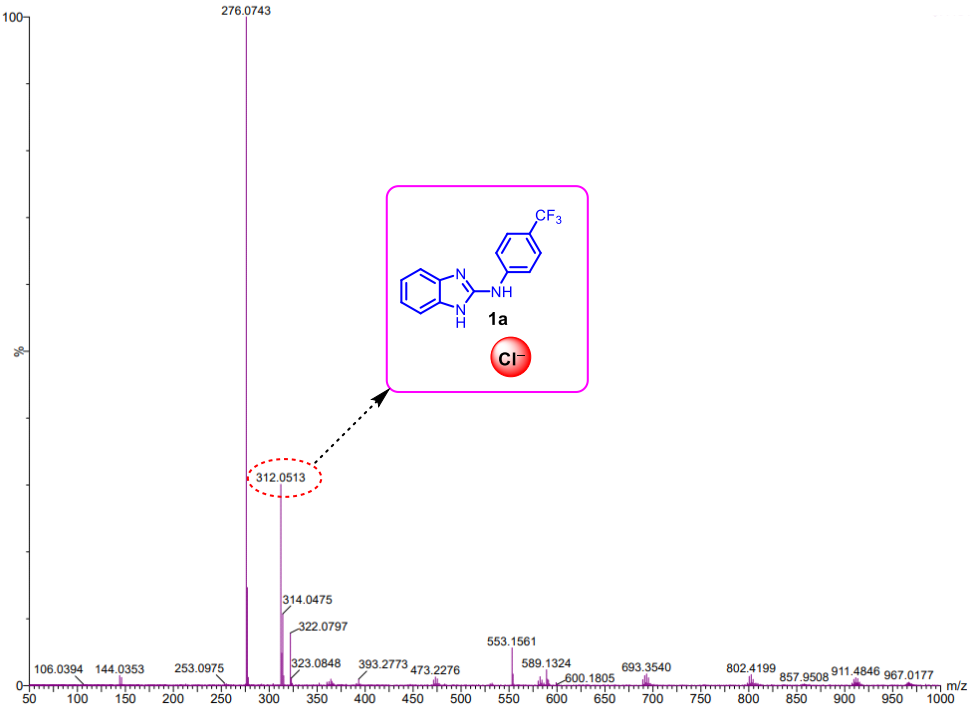

Fig. S30 ESI-MS spectrum of 1:1 mixture of **1a** and TMACl recorded in CH_3CN. The data confirms the presence 1:1 **1a**–Cl^- complex.

VII. Ion transport studies.[S3-S6]

Ion transporting activity studies across EYPC-LUVs⊃HPTS.

Preparation of HEPES buffer and stock solutions: The HEPES buffer of pH = 7.0 was prepared by dissolving an appropriate amount of solid HEPES (10 mM) and NaCl (100 mM) in autoclaved water. The pH was adjusted to 7.0 by addition aliquots from 0.5 M NaOH solution. The stock solution of all carriers was prepared using HPLC grade DMSO.

Preparation of EYPC-LUVs⊃HPTS in NaCl: In 10 mL clean and dry round bottom flask, a thin transparent film of egg yolk phosphatidylcholine (EYPC) was formed using a 1 mL EYPC lipid (25 mg/mL in $CHCl_3$) by providing continuous rotation and purging nitrogen gas. The transparent thin film was completely dried under high vacuum for 4-5 h. After that, the transparent thin film was hydrated with 1 mL HEPES buffer (1 mM HPTS, 10 mM HEPES, 100 mM NaCl, pH = 7.0), and the resulting suspension was vortexed at 10 min intervals during 1 h. This hydrated suspension was subjected to 15 cycles of freeze-thaw (liquid N_2, 55 °C) followed by extrusion through 100 nm (pore size) polycarbonate membrane 21 times to obtain the vesicles of an average 100 nm diameter. The unentrapped HPTS dye was removed by size

exclusion chromatography using Sephadex G-50 (Sigma-Aldrich) with eluting of HEPES buffer (10 mM HEPES, 100 mM NaCl, pH = 7.0). Finally, collected vesicles were diluted to 6 mL to get EYPC-LUVs⊃HPTS. *Final conditions:* ~ 5 mM EYPC, Inside: 1 mM HPTS, 10 mM HEPES, 100 mM NaCl, pH = 7.0, Outside: 10 mM HEPES, 100 mM NaCl, pH = 7.0.

Ion transport activity by HPTS assay: In clean and dry fluorescence cuvette, 1975 μL of HEPES buffer (10 mM HEPES, 100 mM NaCl, pH =7.0) and 25 μL of EYPC–LUVs⊃HPTS vesicle was added. The cuvette was placed in slowly stirring condition using a magnetic stirrer equipped with a fluorescence instrument (t = 0 s). The time-dependent HPTS emission intensity was monitored at λ_{em} = 510 nm (λ_{ex} = 450 nm) by creating pH gradient between intravesicular and extravesicular media by the addition of 0.5 M NaOH (20 μL) at t = 20 s. Then different concentrations of transporter molecules in DMSO were added at t = 100 s. Finally, the vesicles were lysed by the addition of 10% Triton X-100 (25 μL) at t = 300 s to disturb the pH gradient.

The time axis was normalized according to Equation S1:

$$t = t - 100 \qquad \text{Equation S1}$$

The time-dependent data were normalized to percent change in fluorescence intensity using Equation S2:

$$I_F = [(I_t - I_0) / (I_\infty - I_0)] \times 100 \qquad \text{Equation S2}$$

where, I_0 is the initial intensity, I_t is the intensity at time t, and I_∞ is the final intensity after the addition of Triton X-100.

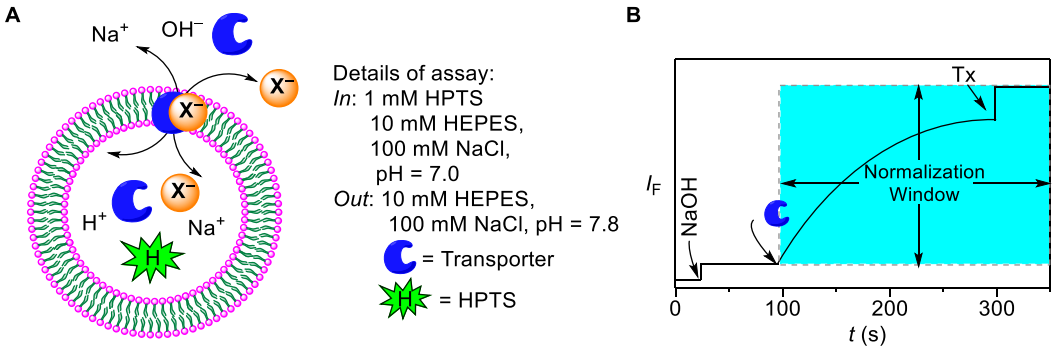

Fig. S31 Representation of fluorescence-based ion transport activity assay using EYPC-LUVs⊃HPTS (A), and illustration of ion transport kinetics showing normalization window (B).

Dose-response activity: The fluorescence kinetics of each transporter at different concentration was studied as a course of time. The concentration profile data were evaluated at t = 290 s to get effective concentration, EC_{50} (i.e. the concentration of transporter needed to achieve 50% chloride efflux)[S7] using Hill equation (Equation S3):

$$Y = Y_\infty + (Y_0 - Y_\infty) / [1 + (c/EC_{50})^n] \qquad \text{Equation S3}$$

where, Y_0 = Fluorescence intensity just before the transporter addition (at t = 0 s), Y_∞ = Fluorescence intensity with excess transporter concentration, c = Concentration of transporter compound, and n = Hill coefficient (i.e., indicative for the number of monomers needed to form an active supramolecule).[S8]

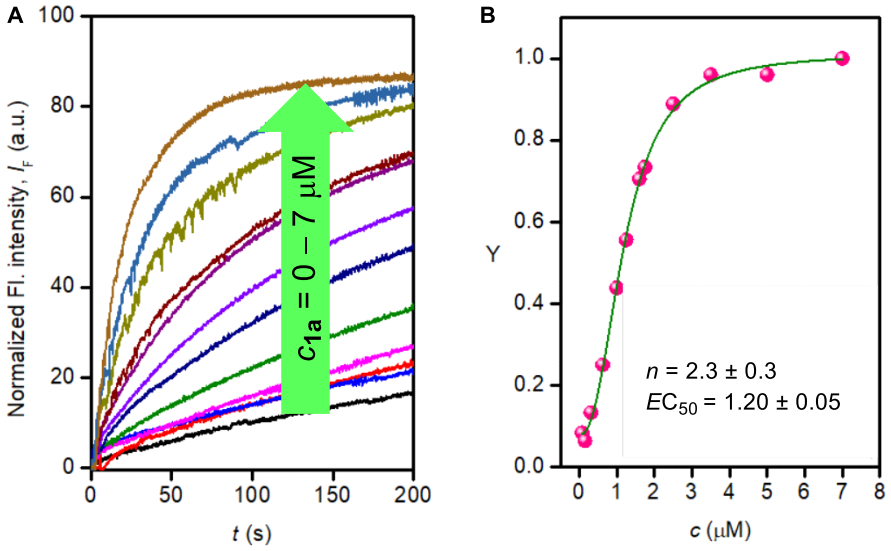

Fig. S32 Concentration-dependent activity of **1a** across EYPC-LUVs⊃HPTS (A). Dose-response plot of **1a** at 180 s after addition of compound (B).

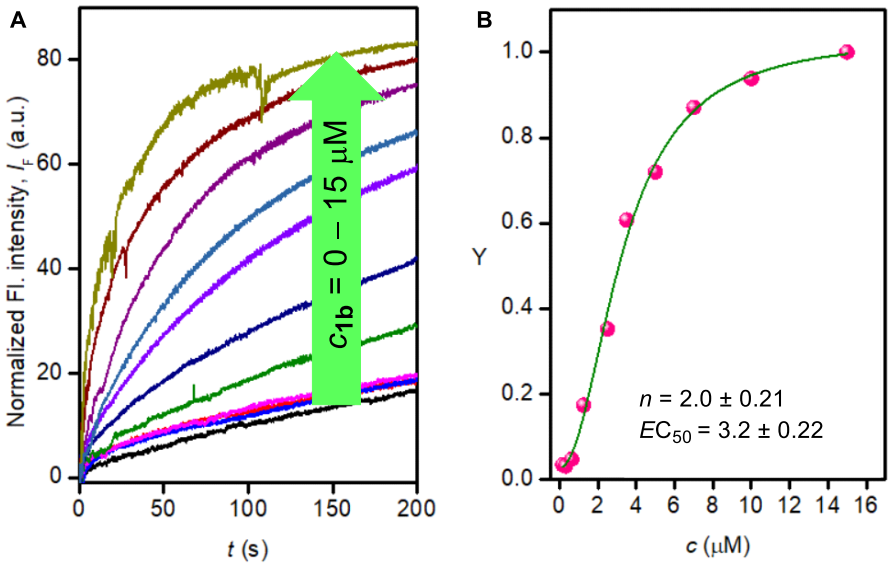

Fig. S33 Concentration-dependent activity of **1b** across EYPC-LUVs⊃HPTS (A). Dose-response plot of **1b** at 180 s after addition of compound (B).

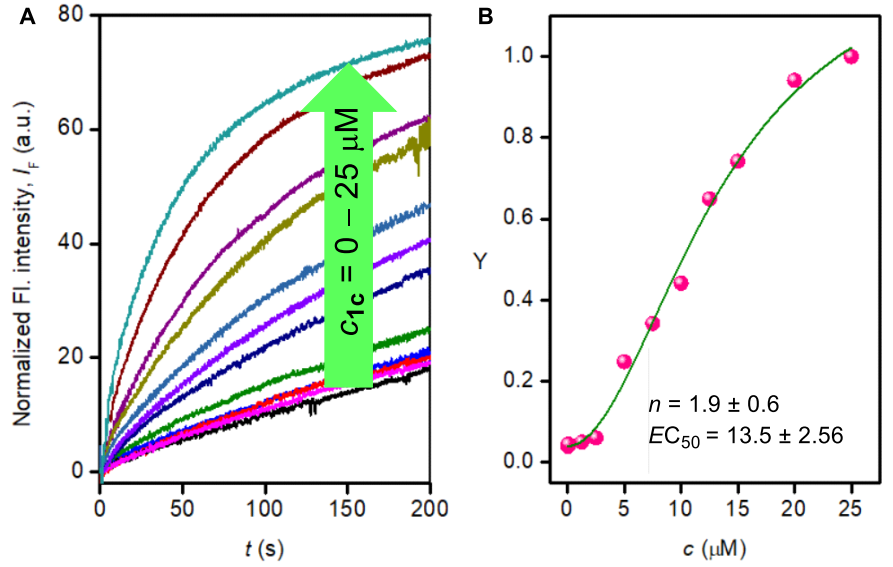

Fig. S34 Concentration-dependent activity of **1c** across EYPC-LUVs⊃HPTS (A). Dose-response plot of **1c** at 180 s after addition of compound (B).

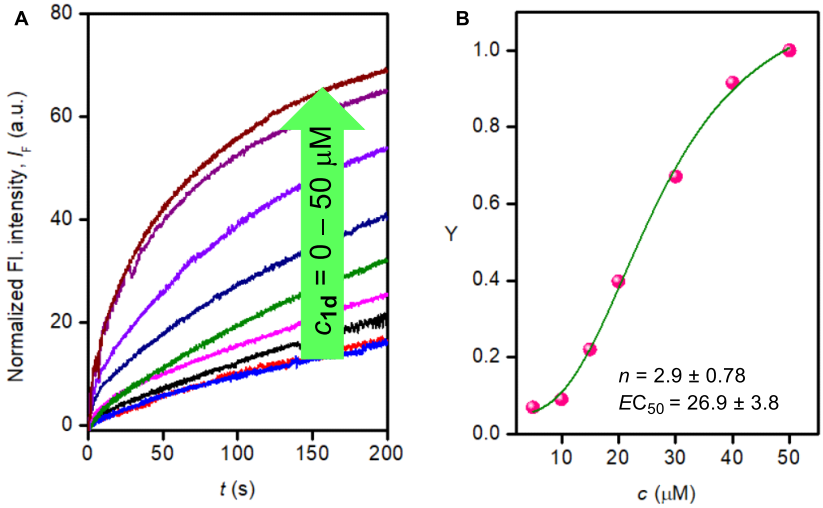

Fig. S35 Concentration-dependent activity of **1d** across EYPC-LUVs⊃HPTS (A). Dose-response plot of **1d** at 180 s after addition of compound (B).

Anion selectivity studies.

Preparation of EYPC-LUVs⊃HPTS for anion selectivity: EYPC-LUVs⊃HPTS (~ 5.0 mM EYPC, inside: 1 mM HPTS, 10 mM HEPES, 100 mM NaCl, pH = 7.0 and outside: 10 mM HEPES, 100 mM NaX, pH = 7.8; where, X^- = Cl^-, Br^-, ClO_4^-, NO_3^- and I^-) were prepared following reported protocol.[S9]

Anion Selectivity Assay: In a clean fluorescence cuvette, 1975 μL of HEPES buffer (10 mM HEPES, 100 mM NaX, at pH = 7.0; where, X^- = Cl^-, Br^-, ClO_4^-, NO_3^- and I^- was added followed by addition of 25 μL of EYPC-LUVs⊃HPTS vesicle in slowly stirring condition by a magnetic stirrer equipped with the fluorescence instrument (at t = 0 s). HPTS fluorescence emission intensity (F_t) was monitored with time at λ_{em} = 510 nm (λ_{ex} = 450 nm). 20 μL of 0.5 M NaOH was added to the cuvette at t = 20 s to make the pH gradient between the intravesicular and extravesicular system. The compound **1a** was added at t = 100 s and at t = 300 s, 25 μL of 10% Triton X-100 was added to lyze all vesicles for the complete destruction of the pH gradient. For data analysis and comparison, time (X-axis) was normalized using Equation S1. Fluorescence intensities (F_t) were normalized to fractional emission intensity I_F using Equation S2.

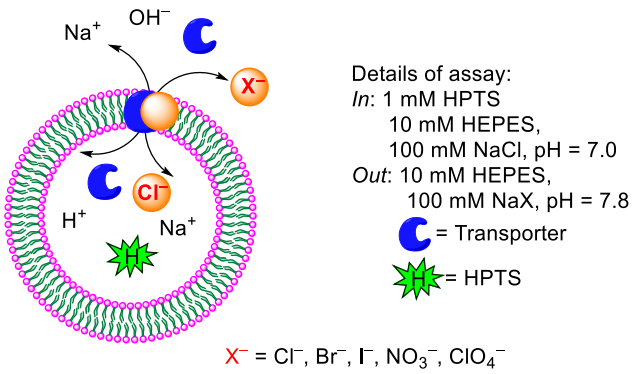

Fig. S36 Schematic representation of fluorescence-based anion assay by changing intravesicular as well as extravesicular anions.

Cation selectivity assay: Similarly, cation selectivity of transporter **1a** was explored by changing extravesicular HEPES buffer solution (10 mM HEPES, 100 mM MCl, pH = 7.0) of chloride salts (MCl) of different cations (M = Li^+, Na^+, K^+, Rb^+, and Cs^+). The time axis was normalized according to Equation S1. The fluorescence data were normalized to percent change in intensity as a course of time using Equation S2.

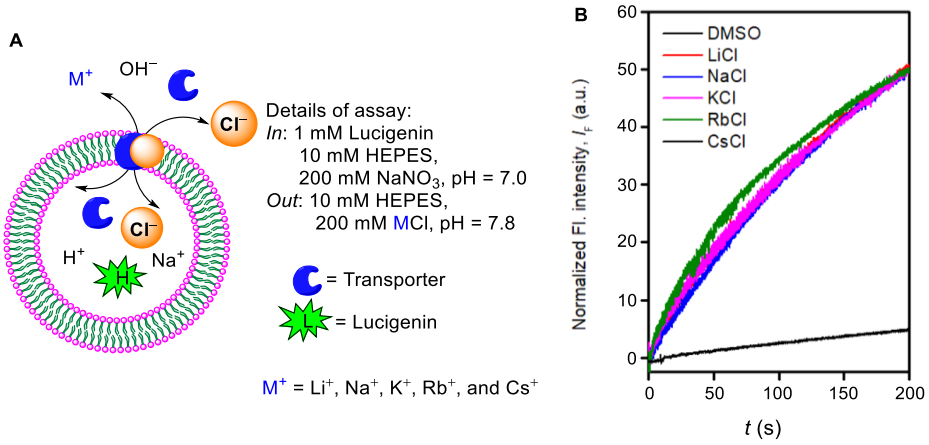

Fig. S37 Schematic representation of fluorescence-based cation selectivity assay (A). Cation selectivity of **1a** (2.0 μM) measured by varying external cations (M^+ = Li^+, Na^+, K^+, Rb^+, Cs^+) across EYPC-LUVs⊃HPTS (B), each bar graph represents mean ion transport activity, calculated from three independent experiments.

Chloride transport activity across EYPC-LUVs⊃lucigenin vesicles.

Preparation of EYPC-LUVs⊃lucigenin vesicles: In 10 mL clean and dry round bottom flask, a thin transparent film of egg yolk phosphatidylcholine (EYPC) was formed by drying 1.0 mL egg yolk phosphatidylcholine (EYPC, 25 mg/mL in $CHCl_3$) with providing continuous rotation

and purging nitrogen. The transparent thin film was kept under the high vacuum for 4 hours to remove all traces of $CHCl_3$. Then the transparent thin film was hydrated with 1.0 mL aqueous $NaNO_3$ (200 mM, 1.0 mM lucigenin) with occasional vortexing at 10 min intervals for 1 h. The resulting suspension was subjected to freeze and thaw cycles (≥ 15, liquid nitrogen, 55 °C water bath) and 21 times extrusion through 200 nm pore size polycarbonate membrane. The size exclusion chromatography (using Sephadex G-50) was performed to remove extravesicular dye using 200 mM $NaNO_3$ solution as eluent. The collected vesicles suspension was diluted to 4 mL. Inside: 200 mM $NaNO_3$, 1 mM lucigenin, pH = 7.0; outside: 200 mM $NaNO_3$, pH = 7.0.

Ion transport activity by lucigenin assay.

In a clean and dry fluorescence cuvette, 200 mM $NaNO_3$ (1975 μL) and EYPC-LUVs⊃lucigenin (25 μL) were taken. This suspension was placed in a slowly stirring condition in a fluorescence instrument equipped with a magnetic stirrer (at t = 0 s). The fluorescence intensity of lucigenin was monitored at λ_{em} = 535 nm (λ_{ex} = 455 nm) as a course of time. The chloride gradient was created by the addition of 2.0 M NaCl (33.3 μL) at t = 20 s between intravesicular and extravesicular system, followed by the addition of the transporter at t = 100 s. Finally, vesicles were lysed by the addition of 10% Triton X-100 (25 μL) at t = 300 s for the complete destruction of the chloride gradient.

The time axis was normalized according to Equation S1 and the time-dependent data were normalized to percent change in fluorescence intensity using Equation S4:

$$I_F = [(I_t - I_0) / (I_\infty - I_0)] \times (-100) \qquad \text{Equation S4}$$

where, I_0 is the initial intensity, I_t is the intensity at time t, and I_∞ is the final intensity after the addition of Triton X-100.

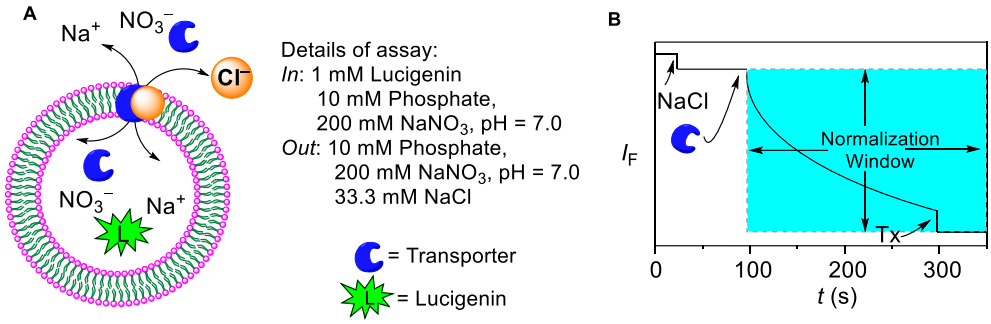

Fig. S38 Representations of fluorescence-based ion transport activity assay using EYPC-LUVs⊃lucigenin (A), and illustration of ion transport kinetics showing normalization window (B).

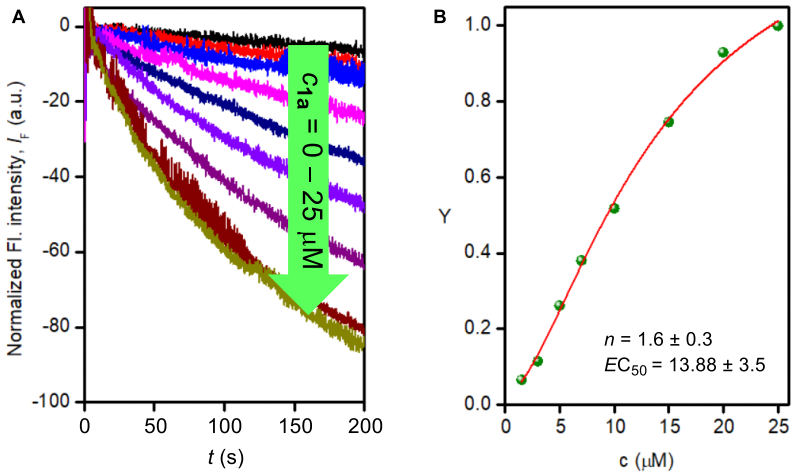

Fig. S39 Concentration-dependent activity of **1a** across EYPC-LUVs⊃lucigenin (A). Dose-response plot of **1a** at 180 s after addition of compound (B).

Ion transport studies through chloride-based ion selective electrode.

Preparation of ISE vesicles: A chloroform solution (1 mL) of 1-palmitoyl-2-oleoylphosphatidylcholine (EYPC) (25 mg) was evaporated under reduced pressure to give a thin film. The lipid film was dried under a high vacuum for 4 hours. The thin film was rehydrated by vortexing with a potassium chloride solution (500 mM KCl, 5 mM phosphate buffer at pH = 7.2). The lipid suspension was then subjected to fifteen freeze-thaw cycles and was allowed to age for 1 h at room temperature. The suspension was extruded twenty-three times through a 200 nm polycarbonate membrane using an extruder (Avanti, The Mini-Extruder set) to obtain unilamellar vesicles containing KCl (500 mM in 5 mM phosphate buffer at pH = 7.2). Non-encapsulated KCl salts were removed by dialyzing the vesicles three times in a potassium gluconate solution (500 mM, 5 mM phosphate buffer at pH = 7.2).

Ion transport activity in the presence of valinomycin and monensin.

In a clean and dry glass vial, 50 µL of above lipid solution and 1950 µL of 500 mM K-gluconate of respective pH buffer solutions was taken and kept in slowly stirring condition by a magnetic stirrer (at t = 0 s) and chloride efflux was monitored with time. Transporter molecule **1a** as DMSO solution was added at t = 50 s, Monensin and Valinomycin as DMSO solutions were added at t = 10 s and finally at t = 300 s, 25 µL of 10% Triton X-100 was added to lyse those vesicles for 100% chloride influx. The chloride efflux for **1a** was monitored in the presence and absence of Monensin and Valinomycin. The value at 50 seconds was set at 0% chloride efflux and the final chloride reading at 300 s was set as 100% chloride efflux. The time axis was normalized using the Equation S5.

$$t = t - 50 \qquad \text{Equation S5}$$

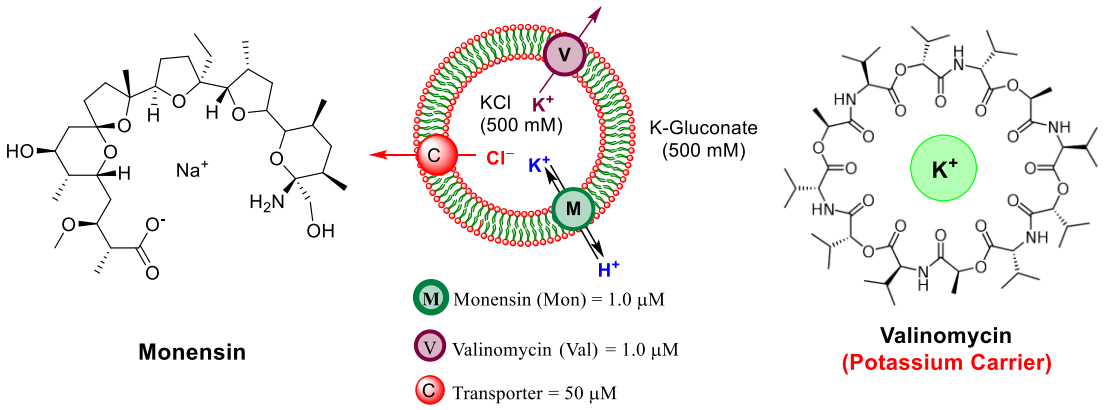

Fig. S40 Schematic representation of ISE-based Valinomycin and Monensin assay.

U-tube experiments for checking Cl^- transport.

These experiments were carried out to check whether the ion transport occurs via a mobile carrier mechanism or through an ion channel formation by the transporter **1a**. In a U-shaped glass tube, 15 mL solution of **1a** (1 mM) and tetrabutylammonium hexafluorophosphate (1 mM) in $CHCl_3$ was placed. Then the left arm (source arm) of the U-tube was filled with a 7.5 mL buffer solution consisting of 500 mM NaCl and 5 mM phosphate buffer set to pH 7.0. On the other hand, the right arm (receiver arm) was filled with a 7.5 mL buffer solution consisting of 500 mM $NaNO_3$ and 5 mM phosphate buffer set to pH 7.0. It is assumed that no ion channel can be formed by **1a** in the organic layer connecting to aqueous layers due to the long path length of the organic layer. Hence, the exchange of Cl^- and NO_3^- ions between two arms would be possible if **1a** functions as a mobile carrier. Therefore the transport of Cl^- ions from the

source to the receiver arm was monitored by a chloride ion selective electrode (ISE) after fixed time intervals for an overall period of 10 days. A control experiment was also done without placing **1a** in the $CHCl_3$ layer. A gradual increase of chloride concentration, only in the presence of **1a**, confirmed the mobile carrier mechanism as the primary transport mechanism.

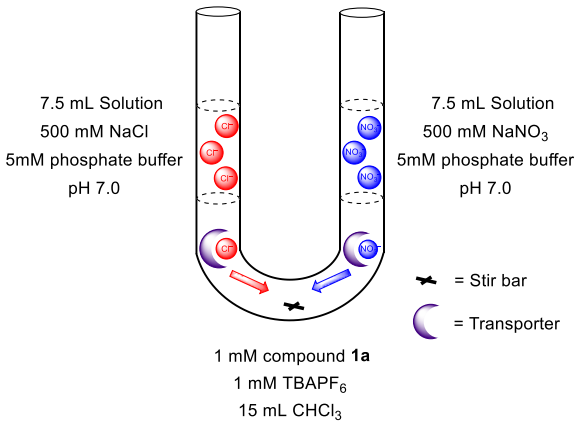

Fig. S41 Schematic representation of U-tube experiment setup.

VIII. Photoresponsive studies.

A. UV-Vis absorbtion studies.

The UV-Vis absorbtion studies of compounds **1a, 2a, 2b, 3a,** and **3b** were carried out in CH_3CN. Initially, stock solutions of these compounds (2 mM in CH_3CN) were prepared in different vials and covered with an aluminum foil.

In a 2 mL UV cuvette, was placed 1900 µL of CH_3CN and 100 µL of either **1a, 2a, 2b, 3a,** or **3b**, was added to get the final concentration of 100 µM. The cuvette was placed in a UV-Vis spectrometer, and the UV-Vis spectrum was recorded.

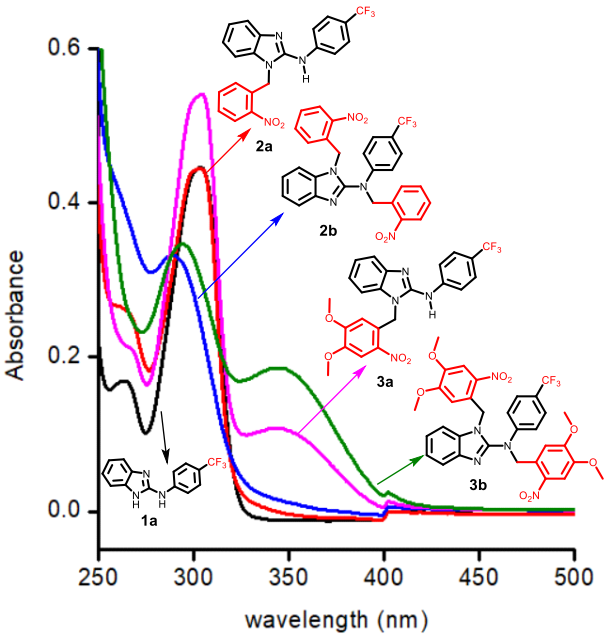

Fig. S42 UV-Vis absorption spectra of compounds **1a, 2a, 2b, 3a,** and **3b**, respectively.

B. Photolytic studies

Assessment of photolysis of procarriers 2a, 2b, 3a, 3b and control compounds 9a, 9b using ^{1}H NMR spectroscopy upon irradiation at 400 nm: In a clean and dry NMR tube, the solution of either **2a**, **2b**, **3a**, **3b**, **9a** or **9b** were taken in DMSO-d_6 (2 mM in 0.5 mL). The ^{1}H NMR spectrum of each sample were recorded first (t = 0 min). Then, the NMR tubes were kept in the photo reactor and irradiated with light of 400 nm using LED (1 × 3.8 Watt) for different time intervals The ^{1}H NMR spectrum of the irradiated samples were recorded at the end of each irradiation. All ^{1}H NMR spectra were processed using MestReNova 6.0 by considering residual solvent peak as an internal reference. Upon photoirradiation, the appearance and disappearance of the different proton peak signals of the procarrier compounds **2a**, **2b**, and **3a**, **3b** indicated the release of as-synthesized active transporter **1a** along with nitrosobenzaldehyde by-products **10a** and **10b**, respectively. On the other hand, the control compounds **9a** and **9b** releases 4-methoxyphenol **8** along with the same by-products **10a** and **10b**.

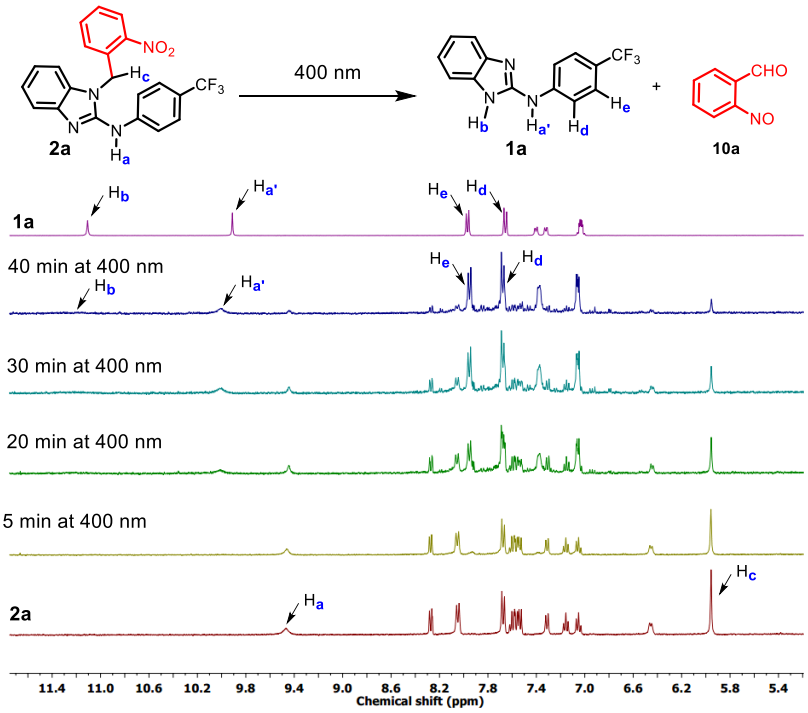

Fig. S43 Phototriggered release of active carrier **1a** from procarrier **2a** monitored by ^{1}H NMR in DMSO-d_6 recorded at different time intervals upon irradiation at 400 nm of electromagnetic radiations using LEDs (1 × 3.8 Watt).

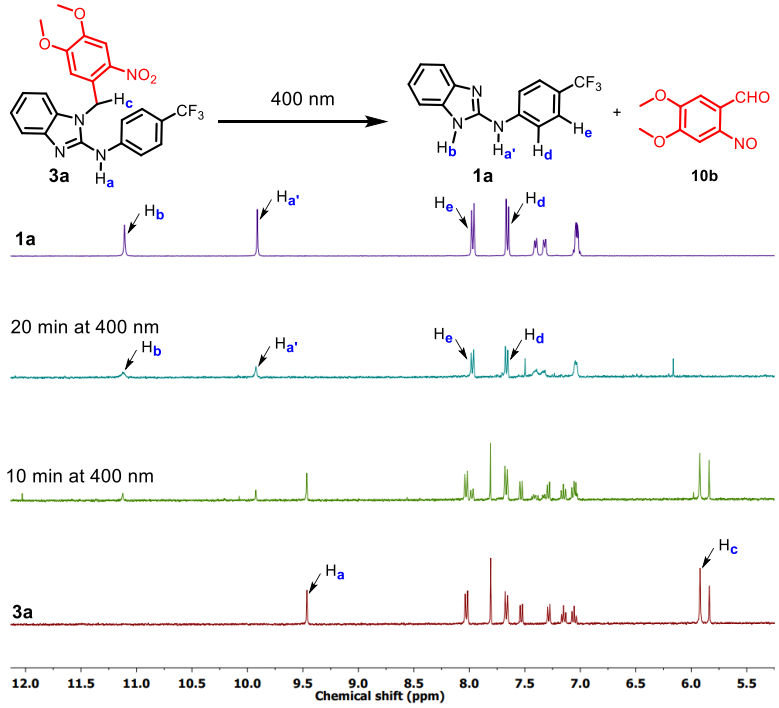

Fig. S44 Phototriggered release of active carrier **1a** from procarrier **3a** monitored by ^{1}H NMR in DMSO-d_6 recorded at different time intervals upon irradiation at 400 nm of electromagnetic radiations using LEDs (1 × 3.8 Watt).

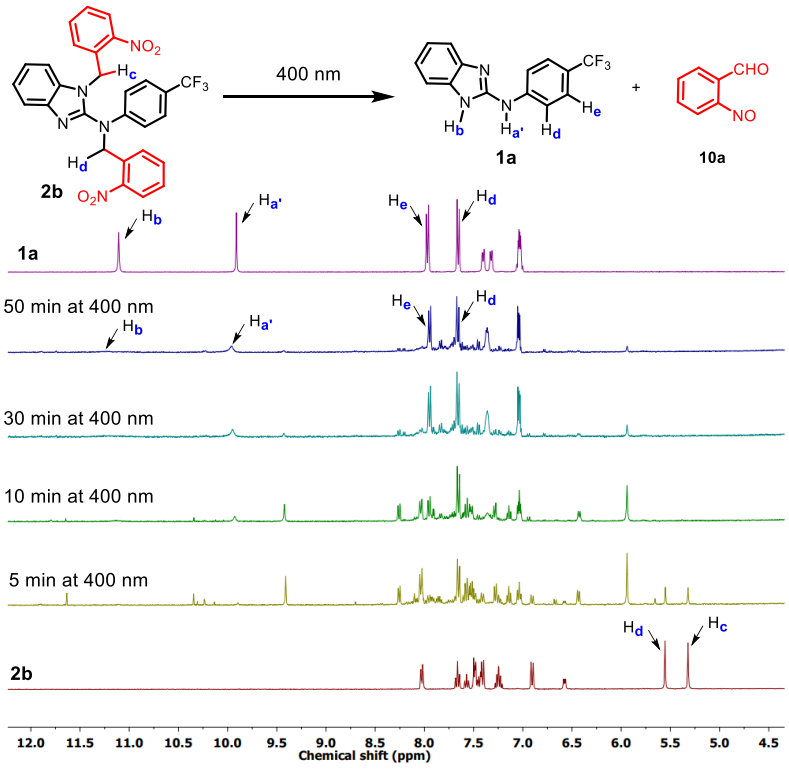

Fig. S45 Phototriggered release of active carrier **1a** from procarrier **2b** monitored by ^{1}H NMR in DMSO-d_6 recorded at different time intervals upon irradiation at 400 nm of electromagnetic radiations using LEDs (1 × 3.8 Watt).

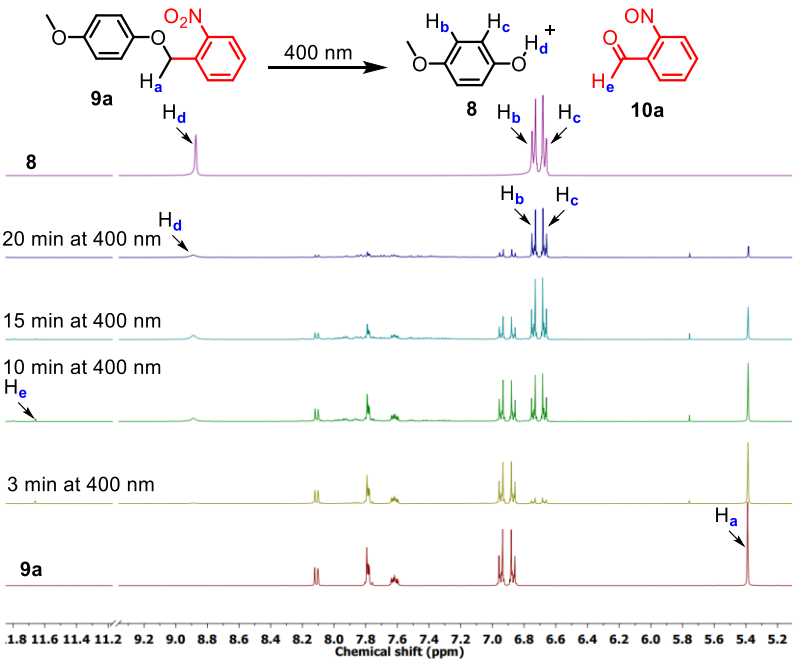

Fig. S46 Photolytic studies of **9a** monitored by ^{1}H NMR in DMSO-d_6 recorded at different time intervals upon irradiation at 400 nm of electromagnetic radiations using LEDs (1 × 3.8 Watt).

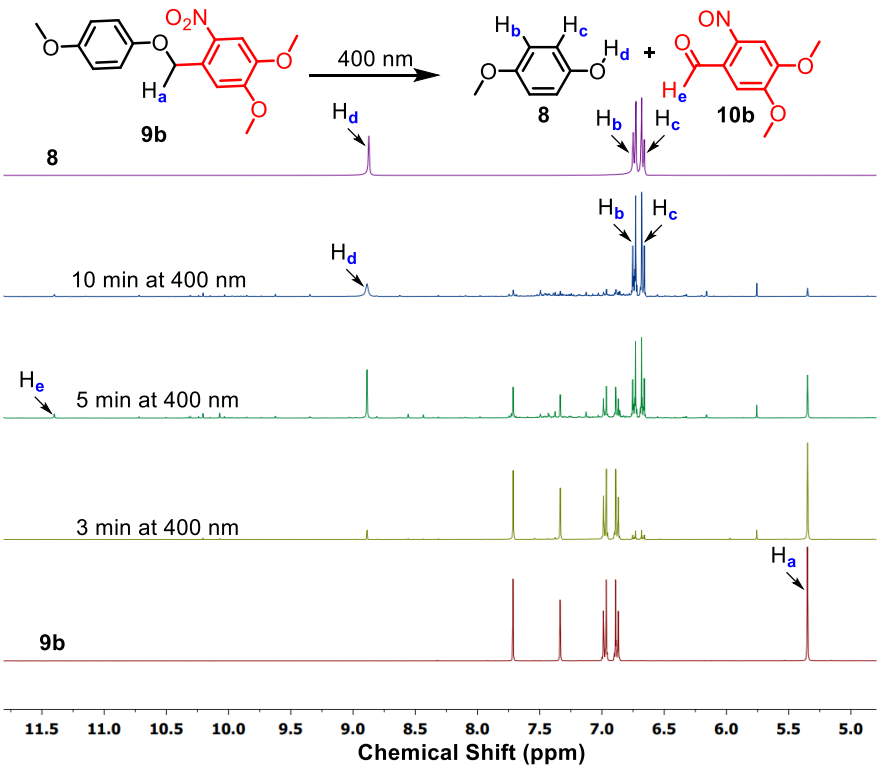

Fig. S47 Photolytic studies of **9b** monitored by ^{1}H NMR in DMSO-d_6 recorded at different time intervals upon irradiation at 400 nm of electromagnetic radiations using LEDs (1 × 3.8 Watt).

IX. Phototriggered ion transport activity across EYPC-LUVs⊃HPTS.

Preparation of EYPC-LUVs⊃HPTS: The vesicles were prepared by the following protocol as stated above.

Phototriggered activation and ion transport assay in LUVs: In clean and dry fluorescence cuvette, 1975 μL HEPES buffer (10 mM HEPES, 100 mM NaCl, pH = 7.0) and 25 μL of vesicles were placed. To this suspension, either **2b**, **3b** (5.0 μM), or **2a**, **3a** (0.2 μM, 1.5 μM, 5.0 μM) were added. The suspension was placed in the fluorescence instrument equipped with a magnetic stirrer and fluorescence intensity of HPTS at λ_{em} = 510 nm (λ_{ex} = 450 nm) was monitored as a course of time *t* by creating a pH gradient across the membrane using NaOH in the extravesicular buffer and, at *t* = 300 s, vesicles were lysed by the addition of 10% Triton X-100 (25 μL) to get the complete destruction of the applied pH gradient. In the next step, the vesicles containing either **2b**, **3b** (5.0 μM), or **2a**, **3a** (0.2 μM, 1.5 μM, 5.0 μM) were initially photoirradiated at 400 nm using LEDs (1 × 3.8 Watt) and subsequently added to the fluorescence instrument to check the ion transport activity after each photoirradiation process.

Significant enhancement in the ion transport activity was observed for the compounds **2b** and **3b** upon photoirradiation and on the other hand, no much difference in the transport activity was observed before and after the photoirradiation for the compounds **2a** and **3a**. The normalized data at 280 s was plotted and compared to show the effect of photoirradiation for ion transport activity as shown in the figures S49A, B and 4C, D. A sample containing 1975 µL HEPES buffer and 20 µL DMSO was also subjected to 10 min irradiation with the same LEDs to see the effect of photoirradiation on the integrity of lipid vesicles.

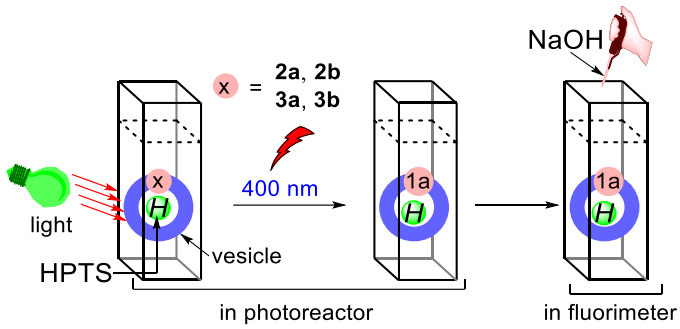

Fig. S48 Description of phototriggered ion transport studies of **2a**, **2b**, **3a**, and **3b**, respectively, upon photoirradiation at 400 nm of light using LEDs (1 × 3.8 Watt).

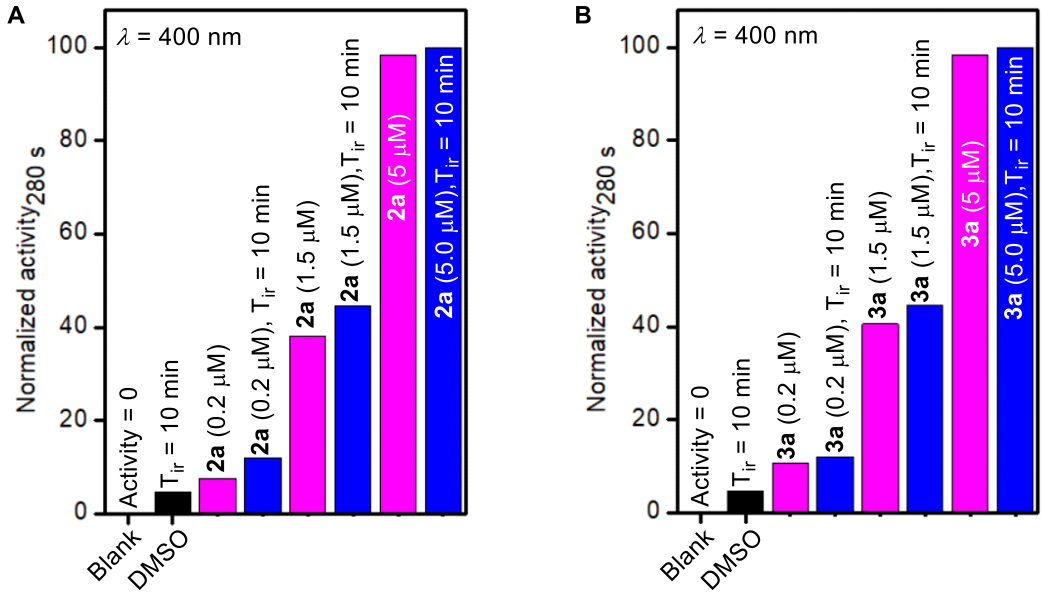

Fig. S49 Normalized ion transport activity data of **2a** (A), and **3a** (B) at different concentrations upon photoirradiation at 400 nm.

X. Theoretical calculations

To get an idea about the conformation of [(**1a**)$_2$+Cl^-], several initial geometries of the complex were generated using the CONFLEX 8 software package[S10, S11] using MMFF94s force field. The calculation provided 10319 conformers. The Boltzmann population of the highest populated conformation (**Conf-1**) was 46.16% and the populations of second to fifth highest conformers (**Conf-2** – **Conf-5**) were 12.12%, 12.11%, 11.57%, 11.55%, respectively (Fig. S51A–E).

Among the several conformations, the highest Boltzmann populated structure was used for geometry optimization. The geometry optimization was carried out by Gaussian 09 program[S12] package using B3LYP functional and 6-31 G(d,p) basis set.[S13] For all structures (i.e., free receptors and anionic complexes), the vibrational frequency calculation during the geometry optimization shows no imaginary frequencies, which indicates that all optimized structures are ground state minima.

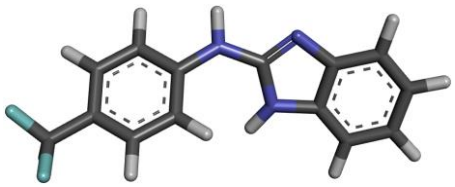

Fig. S50 The geometry optimized structures of **1a**.

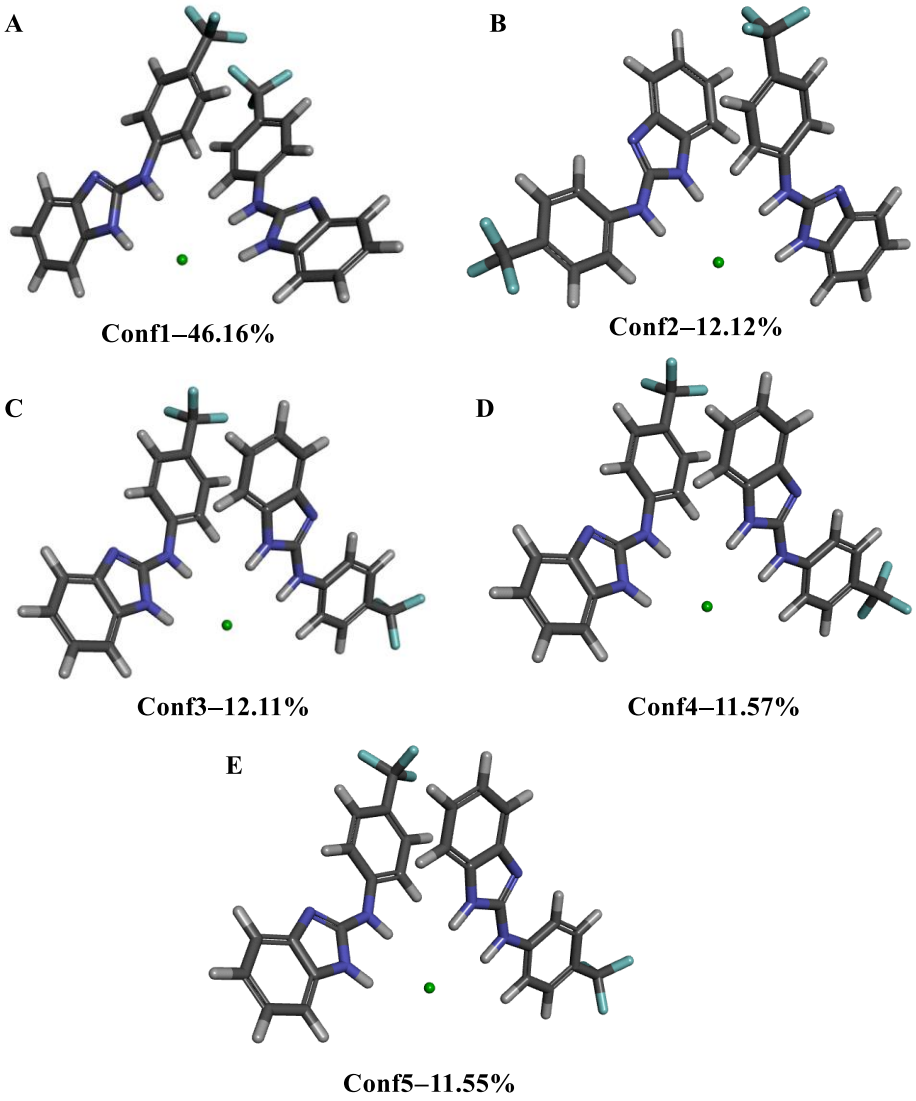

Fig. S51 Initial geometries **Conf-1** – **Conf-5** (A–E) for [(**1a**)$_2$+Cl$^-$], optimized by CONFLEX 8 software using MMFF94s force field.

The Gaussian 09 program was used to calculate the zero-point energy (ZPE) and basis set superposition error (BSSE) corrected bonding energy of [(**1a**)$_2$+Cl$^-$], which was used for the calculation of binding energy (*BE*) using the following equations.

$$BE = [HF_{[\mathbf{M}+Cl^-]} + ZPE_{[\mathbf{M}+Cl^-]} + BSSE_{[\mathbf{M}+Cl^-]}] - 2 \cdot [HF_{\mathbf{M}} + ZPE_{\mathbf{M}}] - [HF_{Cl^-}] \qquad \text{Equation S6}$$

where, M is the receptor (i.e. **1a**), $HF_{[\mathbf{M}+Cl^-]}$ = electronic energy of [(**1a**)$_2$+Cl$^-$] complex, $ZPE_{[\mathbf{M}+Cl^-]}$ = zero point energy of [(**1a**)$_2$+Cl$^-$] complex, $BSSE_{[\mathbf{M}+Cl^-]}$ = BSSE of [(**1a**)$_2$+Cl$^-$] complex, $HF_{\mathbf{M}}$ = electronic energy of the receptor M, $ZPE_{\mathbf{M}}$ = zero point energy of the receptor **M**, HF_{Cl^-} = electronic energy of anion Cl$^-$.

The structures (i.e., free receptor and the complex), the vibrational frequency calculated during the geometry optimization, shows no imaginary frequencies, which indicates that all optimized structures are ground state minima.

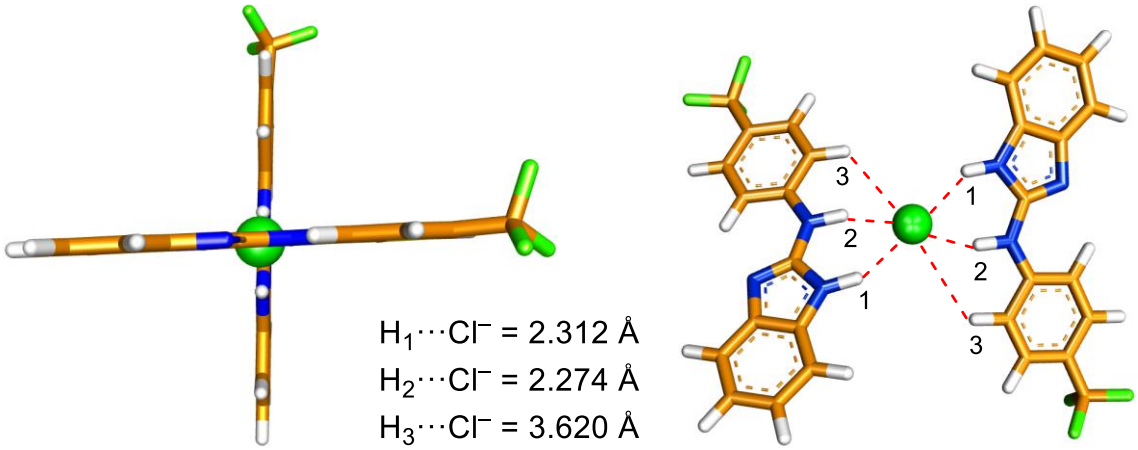

Fig. S52 Two different modes of geometry optimized structures of (**1a**)$_2$·Cl$^-$.

Table S1. The electronic energy (HF), zero point energy (ZPE), basis set superposition error (BSSE) corrected energy (in Hartree unit) for all structures and complexes are calculated at the DFT B3LYP/6-31G(d,p) level of theory.

Structures	Energy values
$HF_{[\mathbf{M}+Cl^-]}$ (in Hartree)	–2467.0444543
$ZPE_{[\mathbf{M}+Cl^-]}$ (in Hartree)	0.4435059
$BSSE_{[\mathbf{M}+Cl^-]}$ (in Hartree)	0.00991909
$HF_{\mathbf{M}}$ (in Hartree)	–1003.3357982
$ZPE_{\mathbf{M}}$ (in Hartree)	0.2209569
HF_{Cl^-} (in Hartree)	–460.2522333
BE (in Hartree)	–0.10911337
BE (in kcal/mol)	–68.4696273

Table S2. Atomic coordinates of the optimized structure of lowest energy conformation obtained for **1a** from DFT B3LYP/6-31g (d,p) geometry optimization.

Charge = 0, Multiplicity = 1

Atom #	Atom Type	x	y	z
1	C	5.566242	1.641624	0.234188
2	C	6.125590	0.415974	-0.167275
3	C	5.333760	-0.711320	-0.379317
4	C	3.955005	-0.594755	-0.178534
5	C	3.411079	0.648837	0.222803
6	C	4.191526	1.781496	0.433092
7	N	2.950211	-1.545564	-0.320075
8	C	1.847534	-0.908794	-0.007096
9	N	2.038771	0.420716	0.312179
10	N	0.621759	-1.536548	0.061080
11	H	0.704921	-2.543121	0.047150
12	C	-0.661815	-0.993942	0.007615
13	H	1.354494	1.027156	0.735806
14	C	-0.929589	0.296247	-0.485356
15	C	-2.234799	0.778335	-0.507543
16	C	-3.296114	-0.011373	-0.062440
17	C	-3.037198	-1.304572	0.404367
18	C	-1.738167	-1.789356	0.443984
19	C	-4.692196	0.537958	-0.035801
20	F	-4.889526	1.460488	-1.005023
21	F	-4.975892	1.146434	1.142174

22	F	-5.618337	-0.433618	-0.201901
23	H	6.214369	2.498043	0.392491
24	H	7.199239	0.348652	-0.315021
25	H	5.762812	-1.658383	-0.689234
26	H	3.759639	2.728993	0.740834
27	H	-0.130326	0.901548	-0.896082
28	H	-2.431512	1.769816	-0.900885
29	H	-3.856726	-1.931311	0.738670
30	H	-1.543451	-2.789522	0.820613

Table S3. Atomic coordinates of the optimized structure of lowest energy conformation obtained for [(**1a**)$_2$+Cl$^-$] complex from DFT B3LYP/6-31G (d,p) geometry optimization.

Charge = –1, Multiplicity = 1

Atom #	Atom Type	x	y	z
1	Cl	0.000000	0.000000	0.986720
2	C	-4.001572	5.180677	4.104000
3	C	-4.091698	3.825650	4.464391
4	C	-3.306785	2.854556	3.837202
5	C	-2.434794	3.289863	2.842585
6	C	-2.330501	4.655231	2.465259
7	C	-3.125286	5.609983	3.106007
8	N	-1.531744	2.628937	2.031196
9	C	-0.946583	3.588053	1.232924
10	N	-1.391108	4.811827	1.455407
11	N	0.000000	3.180256	0.327170

12	H	0.182745	2.171871	0.339623
13	C	0.723357	3.942261	-0.577830
14	H	-1.296164	1.635363	1.984267
15	C	0.586010	5.338350	-0.711478
16	C	1.355526	6.019247	-1.647969
17	C	2.270794	5.345524	-2.462376
18	C	2.407203	3.957816	-2.329421
19	C	1.647719	3.264066	-1.400865
20	H	-0.118910	5.857685	-0.075835
21	C	3.043542	6.081078	-3.507977
22	F	4.255608	5.518029	-3.744157
23	F	3.265844	7.376520	-3.171040
24	F	2.405608	6.110678	-4.710278
25	H	-4.627855	5.908053	4.613722
26	H	-4.784398	3.524756	5.245458
27	H	-3.374897	1.806879	4.114118
28	H	-3.053441	6.656312	2.825142
29	H	1.248263	7.095232	-1.740789
30	H	3.117990	3.423006	-2.950765
31	H	1.759956	2.188702	-1.295922
32	C	4.001572	-5.180677	4.104000
33	C	4.091698	-3.825650	4.464391
34	C	3.306785	-2.854556	3.837202
35	C	2.434794	-3.289863	2.842585

36	C	2.330501	-4.655231	2.465259
37	C	3.125286	-5.609983	3.106007
38	N	1.531744	-2.628937	2.031196
39	C	0.946583	-3.588053	1.232924
40	N	1.391108	-4.811827	1.455407
41	N	0.000000	-3.180256	0.327170
42	H	-0.182745	-2.171871	0.339623
43	C	-0.723357	-3.942261	-0.577830
44	H	1.296164	-1.635363	1.984267
45	C	-1.647719	-3.264066	-1.400865
46	C	-2.407203	-3.957816	-2.329421
47	C	-2.270794	-5.345524	-2.462376
48	C	-1.355526	-6.019247	-1.647969
49	C	-0.586010	-5.338350	-0.711478
50	H	-1.759956	-2.188702	-1.295922
51	C	-3.043542	-6.081078	-3.507977
52	F	-4.255608	-5.518029	-3.744157
53	F	-3.265844	-7.376520	-3.171040
54	F	-2.405608	-6.110678	-4.710278
55	H	4.627855	-5.908053	4.613722
56	H	4.784398	-3.524756	5.245458
57	H	3.374897	-1.806879	4.114118
58	H	3.053441	-6.656312	2.825142
59	H	-3.117990	-3.423006	-2.950765

60	H	-1.248263	-7.095232	-1.740789
61	H	0.118910	-5.857685	-0.075835

XI. Biological studies

Cell culture protocol:[S14] The MCF 7 cells were grown in high glucose Dulbecco's Modified Eagle Medium (DMEM; Lonza) containing 2 mM L-glutamine. The media was supplemented with 10% (v/v) heat-inactivated fetal bovine serum (FBS; Invitrogen) and 100 units/mL penicillin-streptomycin (Invitrogen). Cells were maintained in 100 mm tissue culture treated dishes (Eppendorf) at 37 °C in humidified 5% CO_2 incubator (Thermo Scientific).

MTT-based cytotoxicity assay: The cells were dispersed in a 96-well flat bottom tissue culture treated plates (Eppendorf) at density of 8000 cells/well (per 100 µL) and incubated at 37^{o}C in a humidified 5% CO_2 incubator for 24 h. Compounds were added to each well at the required concentrations maintaining maximum amount of DMSO at 1 µL. Following 24 h incubation at 37^{o}C the media was aspirated out and replaced with 110 µL of MTT solution (0.5 mg/mL) in DMEM and incubated for 4 h in identical conditions. Then the media was removed and 100 µL of DMSO was added in each well to dissolve the formazan crystals. The absorbance was recorded in a Varioskan Flash (Thermo Scientific) multimode plate reader at 570 nm wavelength. All experiments were performed in triplicate, and the relative cell viability (%) was expressed as a percentage of vehicle (DMSO- 1 µL) treated control.

Phototriggered protransporter activation in cells: MCF 7 were dispersed in a 96-well flat bottom tissue culture treated plates (Eppendorf) in complete L-15 medium at a density of 8000 cells/well (per 100 µL) and incubated at 37^{o}C in a 5% CO_2 incubator for 24 h. The cells were then treated with compounds **2b** and **3b** (in DMSO) at different concentrations, maintaining a maximum amount of DMSO at 1 µL per well, and the plate was irradiated for 20 min at 400 nm using a high-power LED (~3.8 W radiant flux, plate positioned at a distance of 8 cm from LED). The plate was then incubated for 24 h at 37°C (5% CO_2). Post incubation, the media was aspirated out and replaced with 110 µL (per well) of MTT solution (0.5 mg/mL) in DMEM. Following incubation at 37°C (5% CO_2) for 4 h, the media was removed and the formazan crystals formed were dissolved using 100 µl DMSO. The absorbance for each well was measured at 570 nm using a a Varioskan Flash (Thermo Scientific) multimode plate reader. All

experiments were performed in triplicate, and the relative cell viability (%) was expressed as a percentage of vehicle (DMSO- 1 µL) treated control.

Evaluation of *o*-nitrosobenzaldehyde byproductS (10a and 10b) cytotoxicity: To evaluate the cytotoxicity of the *o*-nitrosobenzaldehyde byproducts **10a** and **10b**, the compounds **9a** and **9b** were used. These compounds upon photoirradiation lead to the formation of *p*-methoxyphenol **8** and *o*-nitrosobenzaldehyde byproducts **10a** and **10b** as are yielded by the photoirradiation of **2b** and **3b** respectively. The protocol followed was same as the modified MTT assay for assessment of *in vitro* photoactivation of protransporters described previously.

XII. References

S1. *http://app.supramolecular.org/bindfit/*, (accessed July 2017).

S2. P. Thordarson, *Chem. Soc. Rev.*, 2011, **40**, 1305-1323.

S3. T. Saha, S. Dasari, D. Tewari, A. Prathap, K. M. Sureshan, A. K. Bera, A. Mukherjee and P. Talukdar, *J. Am. Chem. Soc.*, 2014, **136**, 14128-14135.

S4. P. Talukdar, G. Bollot, J. Mareda, N. Sakai and S. Matile, *J. Am. Chem. Soc.*, 2005, **127**, 6528-6529.

S5. V. Gorteau, G. Bollot, J. Mareda, A. Perez-Velasco and S. Matile, *J. Am. Chem. Soc.*, 2006, **128**, 14788-14789.

S6. T. Saha, M. S. Hossain, D. Saha, M. Lahiri and P. Talukdar, *J. Am. Chem. Soc.*, 2016, **138**, 7558-7567.

S7. A. Vargas Jentzsch, D. Emery, J. Mareda, P. Metrangolo, G. Resnati and S. Matile, *Angew. Chem. Int. Ed.*, 2011, **50**, 11675-11678.

S8. S. Bhosale and S. Matile, *Chirality*, 2006, **18**, 849-856.

S9. C. Ren, X. Ding, A. Roy, J. Shen, S. Zhou, F. Chen, S. F. Yau Li, H. Ren, Y. Y. Yang and H. Zeng, *Chem. Sci.*, 2018, **9**, 4044-4051.

S10. S. O. H. Goto, N. Nakayama, K. Ohta, CONFLEX 8, CONFLEX Corporation, Tokyo, Japan, 2012.

S11. H. Goto and E. Osawa, *J. Am. Chem. Soc.*, 1989, **111**, 8950-8951.

S12. Gaussian 09, Revision D.01, M. J. Frisch, G. W. Trucks, H. B. Schlegel, G. E. Scuseria, M. A. Robb, J. R. Cheeseman, G. Scalmani, V. Barone, B. Mennucci, G. A. Petersson, H. Nakatsuji, M. Caricato, X. Li, H. P. Hratchian, A. F. Izmaylov, J. Bloino, G. Zheng, J. L. Sonnenberg, M. Hada, M. Ehara, K. Toyota, R. Fukuda, J. Hasegawa, M. Ishida, T. Nakajima, Y. Honda, O. Kitao, H. Nakai, T. Vreven, J. J. A. Montgomery, J. E. Peralta,

F. Ogliaro, M. Bearpark, J. J. Heyd, E. Brothers, K. N. Kudin, V. N. Staroverov, T. Keith, R. Kobayashi, J. Normand, K. Raghavachari, A. Rendell, J. C. Burant, S. S. Iyengar, J. Tomasi, M. Cossi, N. Rega, J. M. Millam, M. Klene, J. E. Knox, J. B. Cross, V. Bakken, C. Adamo, J. Jaramillo, R. Gomperts, R. E. Stratmann, O. Yazyev, A. J. Austin, R. Cammi, C. Pomelli, J. W. Ochterski, R. L. Martin, K. Morokuma, V. G. Zakrzewski, G. A. Voth, P. Salvador, J. J. Dannenberg, S. Dapprich, A. D. Daniels, O. Farkas, J. B. Foresman, J. V. Ortiz, J. Cioslowski, D. J. Fox, Gaussian, Inc., Wallingford CT, **2013**.

S13. A. D. McLean and G. Chandler, *J. Chem. Phys.*, 1980, **72**, 5639-5648.

S14. S. B. Salunke, J. A. Malla and P. Talukdar, *Angew. Chem. Int. Ed.*, 2019, **58**, 5354-5358.